# A De-aggregation strategy based optimal co-scheduling of heterogeneous flexible resources in virtual power plant

Zheng, Zixuan; Li, Jie; Liu, Xiaoming; Huang, Chunjun; Hu, Wenxi; Xiao, Xianyong; Zhang, Shu; Zhou, Yongjun; Yue, Song; Zong, Yi

**DOI**
10.1016/j.apenergy.2025.125404

**Publication date**
2025

**Document Version**
Final published version

**Published in**
Applied Energy

Applied Energy 383 (2025) 125404

Contents lists available at ScienceDirect

Applied Energy

journal homepage: www.elsevier.com/locate/apenergy

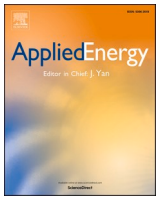

# A De-aggregation strategy based optimal co-scheduling of heterogeneous flexible resources in virtual power plant

Zixuan Zheng [a], Jie Li [a], Xiaoming Liu [b], Chunjun Huang [c], Wenxi Hu [a,*], Xianyong Xiao [a], Shu Zhang [a], Yongjun Zhou [a,b], Song Yue [b], Yi Zong [d]

[a] Department of Electrical Engineering, College of Electrical Engineering, Sichuan University, Chengdu 610000, China
[b] Lhasa Power Supply Company, State Grid Tibet Electric Power Company, Co.Ltd, Lhasa 850000, China
[c] Electrical Sustainable Energy Department, Delft University of Technology, Delft 2600, Netherlands
[d] Department of Wind and Energy Systems, Technical University of Denmark, Lyngby 4000, Denmark

## HIGHLIGHTS

- A de-aggregation strategy for multi-type flexible resources in virtual power plant scheduling for optimal peak shaving.
- Collaborative scheduling and peak shaving strategy applied to grid-connected microgrids for multi-type resources.
- A generalization feature model eliminates heterogeneity and quantifies feature differences effectively.
- Feature matching method can enhance the autonomy of microgrid and complementary response capability of multi-type FRs.
- The VPP credibility and return on investment improve by 2.2% and 6.1% through proposed de-aggregation strategy.

## ARTICLE INFO

*Keywords:*
Virtual power plant
Flexible resources
Feature matching
VPP de-aggregation
Discrete choice model

## ABSTRACT

Virtual power plant (VPP) serves as an effective solution for maintaining internal power balance and participating in external peak shaving auxiliary services within grid-connected microgrid involved in multi-type flexible resources (FRs). However, with increasing prominence of the feature heterogeneity in response behaviors of diverse FRs and their coupling in peak shaving poses challenges in the accurate decomposition of VPP scheduling commands. This paper proposes a de-aggregation strategy, utilizing discrete choice model and feature matching methods, to dynamically sequence FRs responses while optimizing VPP's peak shaving capability. Initially, heterogeneous features are refined and modeled to characterize the response capability of multi-type FRs in meeting the scheduled demand of grid-connected microgrid (SDGM). Subsequently, a feature difference quantification model and matching priority criterion are formulated to describe the feature mapping relationship and guide dynamic decision-making process. On this basis, the multi-type FRs are co-scheduled in the considered VPP to form a dynamic response sequence achieving peak shaving objectives. Case studies based on real data from a region-connected microgrid demonstrate the proposed strategy's performance in improving return on investment by 6.1 %, reducing peak shaving deviation and power exchange with main grid by 70 % and 13.1 %, respectively, and effectively improve the ability of grid-connected microgrid to balance the power and participate in peaking auxiliary services.

## I. Introduction

### A. Background

With a high proportion of renewable energy sources connected to microgrids, enhancing the fully co-scheduling capability of flexible resources (FRs) becomes a necessary measure to maintain the power balance of microgrids [1,2]. However, the heterogeneity [3], decentralization [4], and ubiquity of multi-type FRs pose difficulties in tapping into their co-regulated potential [5]. In view of these problem, a virtual power plant (VPP) provides an effective solution by aggregating multi-type FRs and utilizing advanced information technology [6]. In

* Corresponding author.
*E-mail address:* huwenxi@scu.edu.cn (W. Hu).

https://doi.org/10.1016/j.apenergy.2025.125404
Received 22 October 2024; Received in revised form 30 December 2024; Accepted 17 January 2025
Available online 24 January 2025

**Nomenclature**

*Abbreviations*

| | |
|---|---|
| VPP | Virtual power plant |
| FR | Flexible resource |
| SDGM | Scheduled demand of grid-connected microgrid |
| FLs | Flexible loads |
| MILP | Mixed integer linear programming |
| ES | Energy storage |
| PSAS | Peak shaving auxiliary service |
| PV | Photovoltaic |
| TL | Transferable load |
| RL | Reducible load |
| AL | Adjustable load |

*Parameters*

| | |
|---|---|
| $\Phi_m$ | Feature matrix of FRs set |
| $E_m$ | Response capacity vector of FRs |
| $R_m$ | Response rate vector of FRs |
| $L_m$ | Response time vector of FRs |
| $Q_m$ | Response potential vector of FRs |
| $C_m$ | Response cost vector of FRs |
| $\theta_m$ | Feature matrix of FRs |
| $\Psi_t$ | Feature matrix of SDGM set |
| $\mathcal{P}$ | Aggregated feasible region of the VPP |
| $P_m$ | Response power of FRs |
| $P_S$ | Maximum response power of FRs |
| $c_m$ | Unit response cost of FRs |
| $P_{SDGM}$ | Power of SDGM |
| *Pfc Wind* | Wind forecasting output power |
| *Pfc PV* | PV forecasting output power |
| $P_{\text{load}}$ | Load forecasting power |
| $Y$ | Risk preference coefficient |
| *Pmax SDGM* | Maximum power of SDGM |
| $c_{SDGM}$ | Unit penalty cost of SDGM |
| $\vartheta$ | Feature set |
| $d_{m,t}$ | Difference the features of between FRs and SDGM |
| $f$ | Comprehensive feature difference |
| $\zeta$ | Initial matching degree between FRs and SDGM |
| $\lambda$ | Matching 0–1 state variable |
| $\Gamma$ | Comprehensive matching degree |
| $\xi$ | Matching random term |
| *Pmax ij* | Maximum value of the line power flow |
| $\tau_{Gt,i}$ | Minimum output coefficient of gas turbine $i$ |
| *PN Gt,i* | Rated power of gas turbine $i$ |
| *PN Hy* | Rated power of hydroelectric power unit |
| *Pmax NE* | Maximum power of net exchange power |
| $\alpha_{min}$, $\alpha_{max}$ | Response lower and upper limit coefficients for TLs |
| $\beta$ | Response coefficient for RLs |
| $R_{Gt}$ | Ramp limits of gas turbine |
| $N_{\max}$ | Upper number of reduced regulation times |
| $\gamma_{min}$, $\gamma_{max}$ | Response lower and upper limit coefficients for ALs |
| *PN ES* | Rated power of ES |
| *EN S* | Rated capacity of ES |
| *E0 S* | Initial capacity of ES |

*Decision variables*

| | |
|---|---|
| *Pg Gt,i* | Power of gas turbine units |
| *Pg Hy* | Output of hydroelectric power unit |
| *Pg NE* | Exchange power of tie-lie |
| *Pg FL* | Response power of flexible loads |
| $P_{bid}$ | Peak shaving bidding power |
| $P_{PS}$ | Actual peak shaving output |
| *Pg ES* | Response power of ES |

particular, grid-connected microgrid combined with VPPs can further contribute to participate in peak shaving services as independent entities [7,8]. Unlike the conventional regulation units and demand response, the VPP concentrates on dynamically enveloping operation characteristics of multi-type FRs to form a multi-dimension feasible region [9], and provides its own external characteristics to the power system operator and electricity market operator [10]. The combination of a microgrid and VPP promotes taking advantage of coordinated complementary FRs [11], and interaction with the auxiliary services market [12]. Additionally, the multi-type FRs with heterogeneous features exhibit different supporting effects on the virtual output characteristics and peak shaving capability of VPPs [13]. And the effectiveness of decomposing scheduled demand has a profound impact on peak shaving benefits, peak shaving risk management, and peak shaving bidding capacity. After the VPP receives a scheduling order issued by the electricity market operator, the VPP should de-aggregate the scheduling command to each FR. Fully considering the feature heterogeneity of multi-type FRs contributes to accurately and rapidly decomposing the scheduled demand of grid-connected microgrids (SDGMs) and reduce assessment deviations of VPPs participating in auxiliary services [14].

The existing studies broaden the adjustment boundaries of VPP to enhance power grid flexibility from various perspectives, such as the dynamic feasible region [15], FRs aggregation [16], response capability characterization [17], and so on. Nonetheless, the accuracy and effectiveness of FRs de-aggregation are influenced by the differentiated response capability of multi-type FRs [18], such as response power, capacity, rate, and cost [19]. Meanwhile, the challenge arises in determining the response priority of various FR types dynamically matching different scheduled demands. This challenge primarily stems from limitations in insufficient sharing of feature information between diverse FR types and scheduling commands [20]. In addition to satisfying the internal power supply-demand balance requirements, the grid-connected microgrid combined with VPP participates in peak shaving auxiliary services (PSAS) for the main grid to overcome high electricity curtailment and achieve benefits [21]. A critical consideration in this context is that the response capability of FRs is typically influenced by the coupling between internal power balance and external peak shaving demand for the microgrid. Correspondingly, these response characteristics of multi-type FRs are quite complex and make it difficult to precisely decompose scheduling commands. Addressing the issue of inaccurate scheduling command decomposition is crucial to ensuring the optimal response performance of multi-type FRs, serving as a primary guarantee for VPP participation in PSAS.

## B. Literature review

In the state-of-the-art literature, the focus on the heterogeneity of multi-type FRs within VPPs primarily centers around type and parameter characteristics, aimed at optimizing VPP scheduling [22,23]. In [24], an optimal coalition of heterogeneous distributed energy resources (DERs) is formed in a commercial VPP, based on weekly bilateral contracting, futures-market involvement, and pool participation. Reference [25] develop a simple yet efficient double deep q-network algorithm to address the challenges posed by a large number of complex and heterogeneous DERs with time-varying states. In [26], an innovative peer-to-peer multi-grade energy trading model is established for heterogeneous DERs and flexible demand. In particular, a reliability credit assignment method is developed for differentiate the energy grades, considering the heterogeneity in energy supplying reliability of DERs. In [27], tracking errors stemming from modeling a heterogeneous fleet of

packetized DERs with a group of homogeneous models are analytically derived. This analysis is conducted for relevant packetized energy management information scenarios.

The mismatching between the source and load power is the main reason leading to power imbalance due to the difficulty in tracking load consumption in time for new energy. Sufficient consideration of power matching between power supply and demand can improve the coordinated operation capability of system, and further solve the problem of power deviation caused by heterogeneous feature. In fact, there are still several studies that implicated the source-load matching with partial feature. Ref. [28] propose a coordinated framework for dynamic regulation of source-load interaction characterized by matching coefficient, which can assist in smoothing power fluctuations for the whole system. Based on the state-queuing model of aggregate air conditioning loads, Ref. [29] develops a matching algorithm with minimizing the tracking error for the renewable energy output and the load power, to achieve renewable energy consumption and output tracking. Ref. [30] constructs an interactive decision model for.

source-load matching based on day-ahead and real-time scheduling. In [31], a method to calculate the source-load matching degree for uncertain factors of wind output is proposed to improve the accommodation capacity of wind power. Meanwhile, the source-load timing matching coefficient considering wind power permeability is proposed to quantitatively evaluate the timing matching degree of regional wind power output and load [32]. Ref. [33] proposes the matching characteristics quantified by comprehensive Spearman constant and Euclidean distance to reduce energy consumption cost.

Relying on advantages of internal resource aggregation within VPP, the flexible shaving resources of VPP are explored to participate in PSAS. For example, Ref. [34] sequentially control typical heating, ventilation, and air-conditioning equipment for summer energy peak shaving through VPP. In [35], the proposed approach can effectively characterize the peak-shaving response characteristics of VPP at multiple spatial and temporal scales. Ref. [36] established a coordinated scheduling model between VPP and distribution company to jointly participate in peak shaving and valley filling, and generate the preferable cooperative benefits. In fact, the combination of grid-connected microgrid and VPP can leverage the advantage in resources management and aggregation. Currently, few scholars investigate the mode of grid-connected microgrid combined with VPP participating in PSAS. Among them, Ref. [12,37] compare and analyze the framework microgrid and VPP, such as modeling techniques, solving methods and multi-objective standpoint. And in [38], a concentrated solar power system with a combined cycle power plant is considered to match peak power demand on the grid. Ref. [39] analyzes energy storage system as an important component of microgrid for PSAS. The above literatures have reference significance for investigating grid-connected microgrid as independent entities in the PSAS market. Additionally, de-aggregation capability of multi-type FRs is an important prerequisite of responding to scheduling commands, coordinating the responsiveness of FRs, and ensuring the credibility of VPP to participate in PSAS. In [40], a bi-level dispatch model of VPP is proposed for PSAS in distribution systems, which achieve the de-aggregation of FRs within VPP by bi-level optimization.

### C. Motivation

Table 1 provides an overview of previous studies on the co-scheduling of FRs. However, serval research gaps can be identified, the VPP de-aggregating problems for multi-type FRs mentioned in this paper are described as follows. Firstly, current studies have quite limited consideration for the generalized modeling when implementing heterogeneity of FRs. Although several literatures [22,27] focused on investigating the heterogeneity of DERs in type and parameters, the insufficient consideration for FRs is difficult in reflecting the generalized model of power supply containing all adjustable resources in the power system. Moreover, the feature difference modeling in available literature mostly considers the power or cost difference quantification; the limited features of FRs pose challenges in characterizing their complete attributes. Furthermore, few studies consider source-load matching within FRs, and ignore the matching characteristics from the perspective of power supply side and demand side. While some researches attempt to utilize the matching degree in the proposed matching model, they primarily focus on the source-load tracking evaluation indicator after

**Table 1**
Comparisons between current studies and our work.

| Research | Year | Heterogeneity of FRs | Feature difference modeling | Matching characteristics[1] | Synergies of FRs in VPP | Solving approaches |
|---|---|---|---|---|---|---|
| [29] | 2018 | × | × | Source-load matching | Only temperature control loads | Artificial immune algorithm |
| [6] | 2019 | × | Only cost and power feature | × | Partial FRs | Particle swarm optimization |
| [28] | 2020 | × | × | Source-load tracking | × | MINP |
| [31] | 2020 | × | × | Source-load matching | × | × |
| [40] | 2020 | × | × | × | √ | MILP |
| [27] | 2021 | Heterogeneous DERs | Energy transfer rates difference | Reference tracking | × | Nonlinear multivariate function |
| [17] | 2021 | × | × | × | √ | MILP |
| [18] | 2021 | × | × | × | √ | MILP |
| [32] | 2021 | × | × | Source-load timing matching | × | × |
| [13] | 2021 | × | × | × | Partial FRs | Beetle antenna search algorithm |
| [33] | 2021 | × | Only cost and power feature | Source-load matching degree | × | × |
| [25] | 2021 | × | × | Time priority matching | √ | Double deep q-network |
| [22] | 2022 | Heterogeneous DERs | × | × | √ | MILP |
| [23] | 2022 | Heterogeneous DERs | × | × | √ | Greedy algorithm |
| [34] | 2022 | × | Equivalent ES model | × | Only thermal loads | Sequential control method |
| [35] | 2022 | × | Differentiated decision-making | Scenario-decision-making | Only user loads | Long short-term memory network |
| [26] | 2023 | Heterogeneous DERs | × | P2P trading matching | × | Alternating direction method of multipliers |
| Our work | – | √ | √ | √ | √ | MILP with CVaR |

[1] Reflecting the tracking capability of diverse FRs as power supply for scheduling commands.

optimization, neglecting optimal feasible region construction and accurate scheduling command decomposition. Additionally, the synergies of FRs in VPP mentioned in these studies do not adequately utilize to participate in PSAS of the main grid; these methods primarily address the internal peak shaving of the power grid rather than grid-connected microgrid. Therefore, there remains a lack of de-aggregation strategy for heterogeneous FRs, necessitating the inclusion of a generalized model, feature matching, and optimal peak shaving to decompose scheduling command.

Aiming at addressing the existing research gap, the key novelty of this paper is: the feature matching between multi-type FRs and scheduling command to de-aggregate VPP. In particular, we address the limitations of conventional optimization scheduling that ignores multi-dimension and heterogeneous feature of multi-type FRs, by presenting a feature matching method in microgrid for implementing the scheduling command decomposition and peak shaving services with main grid.

### D. Contributions

The main contributions of this paper can be summarized as follows:

(a) Developing a de-aggregation strategy for multi-type FRs within VPP, aiming to precisely and dynamically match scheduling commands. This strategy incorporates heterogeneous feature matching to minimize electricity curtailment and optimize power exchange.
(b) Conducting a collaborative scheduling of multi-type FRs and a peak shaving mechanism of VPP to reduce the assessment deviation for PSAS.
(c) Validating the effectiveness of the proposed feature matching method using real data from FRs in Northwest China.

The remainder of this paper is organized as follows: In Section II, the modeling of the FRs' heterogeneous feature matching is presented. Section III presents the co-scheduling framework of the feature matching method, and gives the main objectives and constraints of the de-aggregation strategy. Section IV presents results and discussion based on case studies. The conclusion and future work are drawn in Section V.

## II. Modeling of Flexible Resources Feature Matching

The scheduling framework for grid-connected microgrid participation in PSAS in this section is constructed, which serve as the initial phase towards achieving optimal co-scheduling of VPP. Subsequently, the mathematically generalized modeling of heterogeneous feature for multi-type FRs is refined and established. Specifically, the mathematical equations of matching priority resulting from various feature difference are derived. Finally, considering the differentiated response capability of multi-type FRs, the feature mapping between FRs and scheduled demand based on discrete choice model is further established, which to characterize the feature matching and co-scheduling process comprehensively.

### A. Scheduling Framework

The grid-connected microgrid functions as a controllable unit within PSAS, with the transmission power of the tie line as the assessment basis. Initially, ensuring the internal balance between supply and demand is paramount for the microgrid. Subsequently, the surplus regulated capacity is dispatched to the main grid through optimized scheduling. Essentially, VPP leverages the complementary potential of internal FRs to either curtail power supply or sell electricity, thereby fulfilling its the main grid through optimized scheduling. Essentially, VPP leverages the complementary potential of internal FRs to either curtail power supply or sell electricity, thereby fulfilling its own valley filling objectives and engaging in PSAS for the main grid. Broadly speaking, the primary responsibility of the FRs within VPPs is to facilitate PSAS and reap its associated benefits, with the settlement of peak shaving auxiliary costs provided by the main grid. Consequently, constructing a de-aggregation strategy for multi-type FRs within VPPs, while ensuring the fulfillment of scheduled demand for internal power balance and PSAS, emerges as a pivotal challenge.

Combined with Fig. 1, the scheduled processing of VPP considering PSAS for microgrid can be divided into the following steps:

1) The main grid declares the peak shaving demand, resulting from the volatility and uncertainty of new energy, to the peak shaving auxiliary services;
2) VPP declares the bidding capacity and peak shaving period aggregated with multi-type FRs, and obtains the scheduling command for peak shaving demand;
3) VPP quantifies the feature differences between multi-type FRs and scheduled demand, and calculates the response priority of multi-type FRs to achieve co-scheduling;
4) Multi-type FRs de-aggregate the scheduling command of VPP according to the heterogeneous feature matching of multi-type FRs, with the goal of co-scheduling and meeting peak shaving demand;
5) The deviation assessment and transaction settlement are conducted between VPP and the main grid based on the clearance results.

Specifically, the response power domain of VPP aggregated with multi-type FRs in above step 2) can be represented as [41]:

$$\begin{aligned}\mathscr{P}_{agg} &= \left\{P_{agg} \in R^T | b_{\min} \le AP_{agg} \le b_{\max}\right\} \\ &= \left\{P_{agg} \in R^T | \begin{bmatrix} b^{\mathrm{P}}_{\min} \\ b^{\mathrm{E}}_{\min} \end{bmatrix} \le \begin{bmatrix} E \\ A \end{bmatrix} P_{agg} \le \begin{bmatrix} b^{\mathrm{P}}_{\max} \\ b^{\mathrm{E}}_{\max} \end{bmatrix}\right\}\end{aligned} \tag{1}$$

where $\mathscr{P}_{agg}$ is the feasible region of FRs in VPP; $\boldsymbol{P}_{agg}$ is the aggregated regulation power vector of VPP; $R^T$ is the feasible region space of aggregated power in period $T$; $\boldsymbol{b}_{\min}$ and $\boldsymbol{b}_{\max}$ are the regulated boundary vector of VPP; $\boldsymbol{A}$ is a coefficient matrix depicted the relationship between power and energy; $\boldsymbol{E}$ is an identity matrix; $\boldsymbol{bP}$ **min**, $\boldsymbol{bP}$ **max** are the matrix of lower and upper limits of power regulation, respectively; $\boldsymbol{bE}$ **min**, $\boldsymbol{bE}$ **max** are the matrix of lower and upper limits of energy regulation, respectively.

Moreover, the de-aggregation of multi-type FRs for scheduling command in step 4) can be represented as:

$$\begin{cases} P_{com} = I_{m,t} P_{agg} \\ P_{agg} \in \mathscr{P}_{agg} \end{cases} \tag{2}$$

where $\boldsymbol{P}_{com}$ is the scheduling command of microgrid; $\boldsymbol{I}_{m,t}$ is an m-dimensional vector representing the de-aggregation situation, with elements of 0 or 1.

Based on this, the paper concentrates on coordinating the internal power balance and PSAS in grid-connected microgrid, while solving the de-aggregation problem of multi-type FRs for VPP mentioned above.

### B. Feature Matrix of FRs and SDGM

#### 1) Feature Matrix of FRs

In this paper, we consider the multi-type FRs as power supply in the VPP contain: photovoltaic (PV), wind turbine, gas turbine, hydroelectric power unit, tie-line, transferable loads (TLs), reducible loads (RLs), adjustable loads (ALs), and ES, while constructing a feature matrix of FRs' response behaviors by refining response capacity, response rate, response time, response potential, and response cost. A set involved above FRs is as follows:

$$U = \left\{u_m | u_{Wind}\ u_{PV}\ u_{Gt}\ u_{Hy}\ u_{ti}\ u_{tr}\ u_{re}\ u_{ad}\ u_{ES}\right\} \tag{3}$$

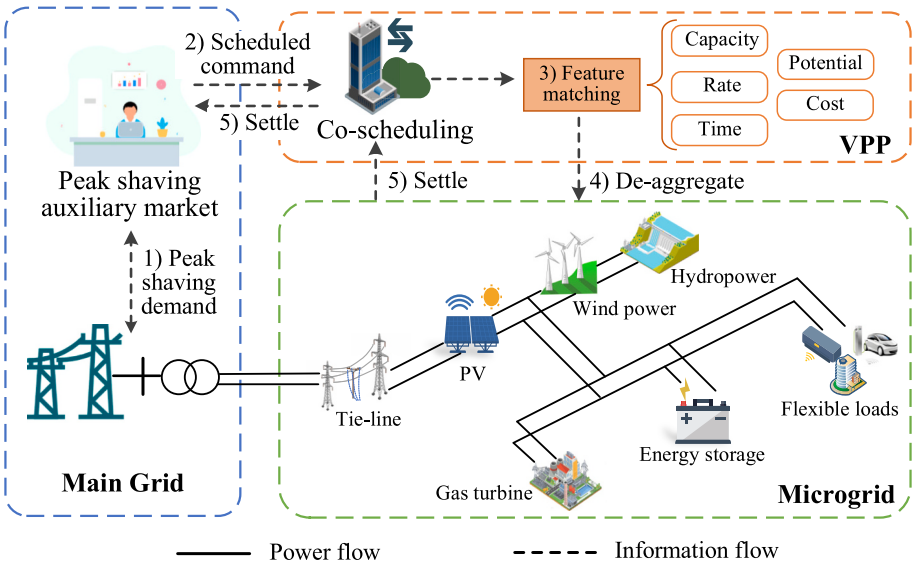


**Fig. 1.** Scheduled framework for microgrid participation in PSAS.

where $U$ is the set of FRs; $u_m$ indicates the any FR in $U$; $u_{Wind}$, $u_{PV}$, $u_{Gt}$, $u_{Hy}$, $u_{ti}$, $u_{tr}$, $u_{re}$, $u_{ad}$, $u_{ES}$ are the wind turbine, PV, gas turbines, hydroelectric power unit, tie-line, TLs, RLs, ALs, and ES, respectively.

The response capacity integrated by response power can be calculated by:

$$E_m = \int_{\Delta t} P_m(t)\Delta t, m \in U \tag{4}$$

where $E_m$ is the response capacity of FR $m$; $P_m(t)$ is the response power of FR $m$ at scheduling time $t$; $\Delta t$ is the temporal resolution.

The response rate of FRs equals to ramp rate, which can be calculated by:

$$R_m = [P_m(t+1) - P_m(t)]/\Delta t, m \in U, t = 1, 2, \ldots, T-1 \tag{5}$$

where $R_m$ is the response rate of FR $m$; $P_m(t+1)$ is the response power at time $t+1$.

The response time of FRs is interval time from scheduling command reception to response, which can be calculated by:

$$L_m = \lceil (t_{m,2} - t_{m,1})/\Delta t \rceil \Delta t, m \in U \tag{6}$$

where $L_m$ is the response time of FR $m$; $t_{m,2}$ is the response time of FR $m$; $t_{m,1}$ is the command reception time of FR $m$.

The primary factors influencing the response potential encompass both down-regulation and up-regulation potentials. Specifically, the up-regulation potential is characterized by the variance between the response power and its minimum value, whereas the down-regulation potential is defined as the variance between the response power and its rated value. The response potential vector is delineated as follows:

$$Q_m = \left(P_m(t) - P_m^{\min}\right)\left(P_m^{\max} - P_m(t)\right), m \in U \tag{7}$$

where $Q_m$ is the response potential of FR $m$; $P\min\ m$ and $P\max\ m$ are the minimum and maximum power of FR $m$, respectively.

The response cost of FRs is primarily composed of response power and unit response costs, in which can be calculated by:

$$C_m = \sum\nolimits_m c_m |P_m(t)|, m \in U \tag{8}$$

where $C_m$ is the response cost of FR $m$; $c_m$ is the unit response cost of FR $m$.

Based on the proposed feature of FRs, the feature matrix of FRs is as follows:

$$\boldsymbol{\Phi}_m = [E_m\ R_m\ L_m\ Q_m\ C_m]^{'} \tag{9}$$

where $\boldsymbol{\Phi}_m$ is the feature matrix of FRs; [•] is the matrix; [•]′ is the transposition of matrix.

In consideration of the nonlinearity inherent in (7), this paper employs the segmented linearization method mentioned in [42] to transform the quadratic function into a segmented linear function with $b$ segments. As a result, (7) can be rewritten as:

$$Q_m = \sum\nolimits_{s=1}^{b} Y_{m,s} p_{m,t,s} + H \tag{10}$$

where $Y_{m,s}$ is the slope of each function segment after segment linearization; $p_{m,t,s}$ is the segmented response power of FRs; $H$ is the response potential of the minimum response power.

Meanwhile, $p_{m,t,s}$ and $H$ satisfy:

$$\begin{cases} H = -P_{m,min}^2 + \left(P_m^{\min} + P_m^{\max}\right)P_{m,min} - P_m^{\min}P_m^{\max} \\ 0 \le p_{m,t,s} \le \left(P_{m,max} - P_{m,min}\right)/b \\ P_m(t) = \sum\nolimits_{s=1}^{b} p_{m,t,s} + P_{m,min} \end{cases} \tag{11}$$

where $P_{m,\min}$ and $P_{m,\max}$ are the segment minimum and maximum value of $P_m(t)$.

2) Feature matrix of SDGM

The SDGM is related to forecasted load power, wind power, and PV output, and denotes the operating baseline declared by the VPP to the electricity market operator as the net load curve. The prediction error of wind and PV output is assumed to follow the normal distribution in this paper, and the probability of scenario $\omega$ is set to $\rho_\omega$. Notably, the response power of multi-type FRs and SDGM are solved in scenario $\omega$, which will not be specially marked in the paper. The SDGM can be calculated by:

$$P_{SDGM}(t) = P_{load}(t) - P_{PV}^{fc}(t) - P_{Wind}^{fc}(t) \tag{12}$$

where $P_{SDGM}(t)$ is the power of SDGM at time $t$ in the region grid, equals to declared operating baseline of VPP at time $t$ based on load forecasted power, wind and PV forecasted output power; $P_{load}(t)$ is the load forecasted power; $Pfc\ PV(t)$ is the forecasted output of PV; $Pfc\ Wind(t)$ is the forecasted wind power.

The set of SDGM is as follows:

$$V = \{v_1, v_2, \ldots v_t, \ldots, v_T\} \tag{13}$$

where $V$ is the set of SDGM; $v_t$ is the SDGM at time $t$, the value of $v_t$ is same as the *Pt peak*.

$$\begin{cases} E_t = \int_{\Delta t} P^g_{SDGM}(t)\Delta t \\ R_t = \left[P^g_{SDGM}(t+1) - P^g_{SDGM}(t)\right]/\Delta t \\ L_t = 0 \\ Q_t = E^g_{SDGM}(t+1) \\ C_t = c_{SDGM}|P^g_{SDGM}(t) - P^g_{im}(t)| \end{cases} \tag{14}$$

where $E_t$, $R_t$, $L_t$, $Q_t$, $C_t$ is the capacity, rate, time, potential, and cost feature of SDGM; $c_{SDGM}$ is the unit benefit of demand assessment reduction; *Pg SDGM*($t$) is the SDGM at time $t$ in microgrid in matching round $g$; *Pg im*($t$) is the imbalance power after optimal operation, the value is equal to *P0 SDGM*($t$) when $g = 0$.

Corresponding to the FRs feature, the generalized features of the peak shaving demand are refined into peaking capacity, peaking rate, peaking time, peaking capacity in next moment, and peaking penalty cost, and the feature matrix of SDGM is as follows:

$$\boldsymbol{\Psi}_t = [E_t\ R_t\ L_t\ Q_t\ C_t]^{'} \tag{15}$$

where $\boldsymbol{\Psi}_t$ is the feature matrix of SDGM.

### C. Feature difference quantification

Based on the above feature matrix of multi-type FRs and SDGM, the basic mathematical principle of matching priority with differentiated feature is derived, as shown in Fig. 2. Firstly, based on the proposed feature of FRs and SDGM containing capacity, rate, time, potential, and cost feature, the matching priority of FRs is derived in Fig. 2 and (16)–(18). Following this, the matching pair of FRs and SDGM at scheduled time $t$ is formed according to Euclidean metric and discrete choice model. Similarly, combined with the proposed five types of FRs features and discrete choice model, the scheduling command is decomposed into the optimal FRs at each scheduled time.

The SDGM is satisfied by diversified response power of FRs, and equals to the sum of response power for FRs. The scheduling command $P_{SDGM}(t)$ can be represented by optimal response power, which can be calculated by:

$$\begin{cases} P_{SDGM}(t) = \sum_m \varpi_m P_{m,0}(t) \\ \sum_m \varpi_m = 1 \\ \varpi \in \{\alpha, \beta, \gamma, \delta, \varepsilon\} \\ m \in U, t \in T \end{cases} \tag{16}$$

where $P_{m,0}(t)$ is the optimal matching response power of FR $m$, $\varpi_m$ is the normalized response power, equal to the ratio of SDGM and optimal matching power as shown in Fig. 2.

A new generalized feature set is obtained by union FRs and SDGM feature, and can be expressed as:

$$\vartheta = \boldsymbol{\Phi}_m \cup \boldsymbol{\Psi}_t = \{E, R, L, Q, C\} \tag{17}$$

where $\vartheta$ is the generalized feature set.

In light of the generalized feature of FRs and SDGM, the feature difference is quantified by the norm. When the optimal feature of FR $m$ aligns with command power of SDGM, the feature difference is deemed as 0. Consequently, The smaller the feature difference, the higher the matching priority of FR $m$. And the feature difference $\Delta\vartheta_{diff}$ and corresponding matching priority are as follows:

$$\begin{cases} \Delta\vartheta_{diff} = \|\vartheta_{SDGM}(t) - \varpi_m\vartheta_{m,0}(t)\| \\ \Delta\vartheta_{diff} = 0, \varpi_m = 1 \\ \Delta\vartheta_{diff,a} \succ \Delta\vartheta_{diff,b}, \varpi_a \succ \varpi_b \\ a, b \in m \end{cases} \tag{18}$$

where $\Delta\vartheta_{diff}$ is the feature difference between multi-type FRs and SDGM; $\vartheta_{SDGM}(t)$ is the feature of SDGM at scheduling time $t$, equals to the function relationship characterized by $P_{SDGM}(t)$. $\vartheta_{m,0}(t)$ is feature of FR $m$ with optimal response power at scheduling time $t$, equals to the function relationship characterized by $P_{m,0}(t)$; $\succ$ represents matching priority

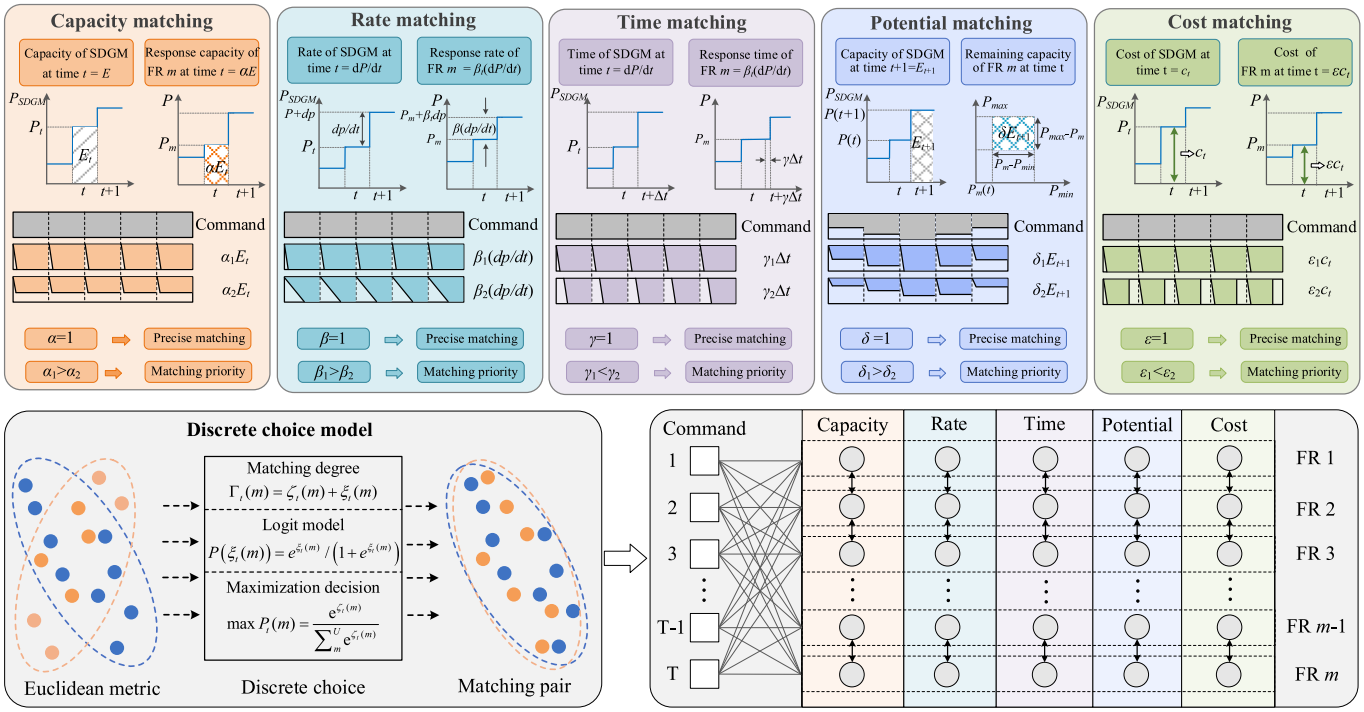


**Fig. 2.** Feature matching characteristics of multi-type FRs.

sequence among multi-type FRs.

The proposed five-type feature differences serve to characterize the responsiveness of FRs to scheduled demand, measuring the difference among the above-mentioned generalized features is the basis for facilitating feature matching. Specifically, the response capacity and potential difference reflect adjusted capability for multi-type FRs to SDGM, the response rate and time difference embody the tracking effect for FRs to SDGM, and the difference between the response cost of FRs and the benefits of peaking demand portrays the scheduling cost of the VPP in matching round. Based on this, the feature differences quantified by Euclidean metric between FRs and SDGM can be expressed as:

$$d_{m,t}(\vartheta) = \sqrt{\sum_{m}^{U}\sum_{t}^{T}\left[\Phi_m(\vartheta) - \Psi_t(\vartheta)\right]^2} \tag{19}$$

where $d_{m,t}$ is the feature difference between FRs and SDGM.

Nevertheless, the non-uniform dimensions among five types of features render them incapable of uniformly quantifying the difference between FRs and SDGM, therefore, they are normalized via range method, which is normalized as follows:

$$d_{m,t}^{`}(\vartheta) = \frac{d_{m,t}(\vartheta) - min\{d_{m,t}(\vartheta)\}}{max\{d_{m,t}(\vartheta)\} - min\{d_{m,t}(\vartheta)\}} \tag{20}$$

where $d^{`}_{m,t}$ is the normalized feature difference.

Therefore, the comprehensive feature differences are linearly weighted by above three indicators and expressed by:

$$f = \sum d_{m,t}^{`}(\vartheta) \tag{21}$$

where $f$ is the comprehensive feature difference.

Based on (21) and adjusted boundary of FRs, FRs timing response sequences can be formulated to cater to peak shaving demand. However, it represents a global optimization strategy that fails to attain the matching sequences to dynamic SDGM.

In this work, an initial match degree is introduced to model the fitness of FRs and SDGM, which can be calculated by:

$$\zeta = \sqrt{1 - f^k} \tag{22}$$

where $\zeta$ is the initial matching degree based on comprehensive feature difference between FRs and scheduled demand; $k$ is the matching coefficient.

## D. Feature matching

Considering the above differentiated feature including capacity, rate, time, potential, and cost feature, different probability combination of multi-type FRs constructs a feasible region $\mathcal{P}$ with various regulated capability as shown in Fig. 3, which can be expressed as:

$$\mathscr{P} = \{\mathbf{\Phi}_m | [E_m\ R_m\ L_m\ Q_m\ C_m]\}, m \in U \tag{23}$$

where $\mathcal{P}$ is the aggregated feasible region of the VPP.

The FRs set $U$ and SDGM set $V$ combine the feature space $F$, this paper defines mapping $\mu$: $U \rightarrow V$ as the matching process between $U$ and $V$ in the feature space $F$, and the mapping satisfies: there is always at least one element $u_m$ corresponding to it in FRs set $U$ for each element $v_t$ in SDGM set $V$, which is as follows:

$$\forall v_t \in V : \exists \mu(u_m) \in v_t, m \geq 0 \tag{24}$$

where $\mu(u_m) \in v_t$ is the matching pair composed by $u_m$ and $v_t$.

Accordingly, the schematic of the projection process can be depicted as Fig. 3. The regulated capability of FRs portrayed by above-mentioned features can form the feasible region of the VPP, which is characterized mathematically as a high-dimensional polytope $\mathcal{P}$. Meanwhile, the feasible region is projected onto the plane $V$ to transform as same dimensional metric space $F$, with the goal of complete overlap. Apparently, the differences in the feasible region represent the response deviation of FRs in the feature space $F$.

Introducing a 0–1 variable $\lambda_t(m)$ to characterize the matching of FRs to SDGM, which is as follows:

$$\lambda_t(m) = \begin{cases} 1, \mu(u_m) \in v_t \\ 0, \mu(u_m) \notin v_t \end{cases} \tag{25}$$

where $\lambda_t(m) = 1$ indicates that FR $m$ matches SDGM at time $t$, $\lambda_t(m) = 0$ indicates that FR $m$ does not match SDGM at time $t$.

In general, meeting scheduled demand across various combinations of multi-type FRs poses a challenge, as the probability combinations may lead to response deviations, manifested as exchange power at the dispatching level.

In econometrics, the discrete choice model (DCM) is commonly used to simulate the choice orientation of decision maker [43]. Similarly, the selection of different flexible resources (FRs) combination according to their feature information is also achieved in a discrete and discontinuous set by dispatching department of power grid [44,45]. According to discrete choice model, the selection behavior of the power grid towards FRs is reflected through the dependent variable and indicator variable. In this study, we opt for the Logit model, with the dependent variable being the peaking scheme, and the indicator variable representing the matching degree of the program (encompassing capacity, rate, time, potential, cost, and random terms).

The comprehensive matching degree function of SDGM $t$ to FR $m$ in the discrete choice model can be expressed as follows:

$$\Gamma_t(m) = \zeta_t(m) + \xi_t(m) \tag{26}$$

where $\Gamma$ is the comprehensive matching degree, characterizes as the

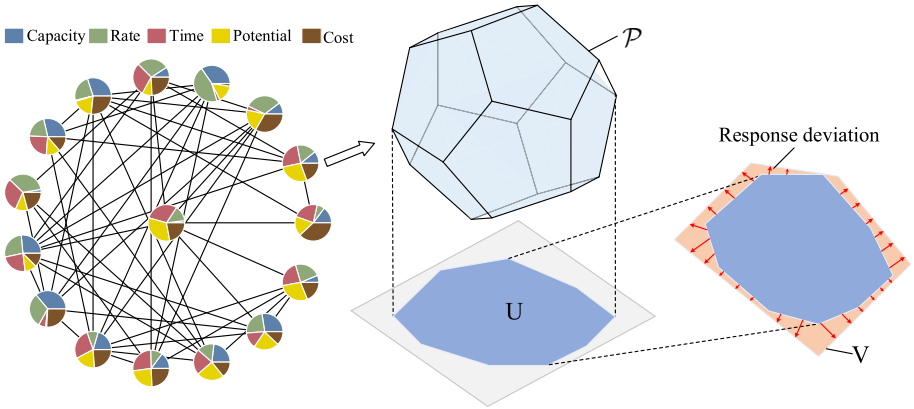


**Fig. 3.** Schematic of high-dimensional polytope projection.

utility value in DCM; $\xi$ is the random perturbed term.

According to the utility-maximizing criterion in the DCM, the FR with the highest matching degree is selected by dispatching center. Therefore, the selection problem for FR is transformed into a probability. Namely, assuming that the matching degree of FR $m$ is higher than FR $h$, the probability of selecting FR $m$ is:

$$\begin{aligned} &P_t(m) = P(\Gamma_t(m) > \Gamma_t(h) \ \ \forall h \neq m) \\ &= P(\zeta_t(m) + \xi_t(m) > \zeta_t(h) + \xi_t(h) \forall h \neq m) \\ &= P(\xi_t(h) - \xi_t(m) < \zeta_t(m) - \zeta_t(h) \forall h \neq m) \end{aligned} \tag{27}$$

where $P_t(m)$, $P_t(h)$ are the probability of choosing FR $m$, $h$ at time $t$, respectively.

Since the Logit model satisfies: 1) Rational decision maker will choose the option that maximizes their utility. 2) the random terms of utility are independent of each other, and obey the extreme value distribution [46]. As a sequence, the probability distribution function $P(\xi_t(m))$ is:

$$P(\xi_t(m)) = e^{\xi_t(m)} / \left(1 + e^{\xi_t(m)}\right) \tag{28}$$

where $P(\xi_t(m))$ is the probability distribution function of random perturbed term $\xi_t(m)$.

Therefore, the selection probability for FR combination is transformed into a probability distribution of the random perturbed term, and combined with (27) and (28), the probability of selecting the FR $m$ can be obtained as:

$$\begin{aligned} P_t(m) &= Pro(\xi_t(h) - \xi_i(m) < \zeta_t(m) - \zeta_t(h) \forall h \neq m) \\ &= \int_{-\infty}^{\zeta_t(m) - \zeta_t(h)} P'(\xi_t(j))\, d\xi_t(j) \\ &= P(\xi_t(j))|_{-\infty}^{\zeta_t(m) - \zeta_t(h)} \end{aligned} \tag{29}$$

Substituting (26) into (29), the $P_t(m)$ is obtained as:

$$\begin{aligned} P_t(m) &= e^{\zeta_t(m) - \zeta_t(h)} / \left(1 + e^{\zeta_t(m) - \zeta_t(h)}\right) \\ &= e^{\zeta_t(m)} / \left(e^{\zeta_t(m)} + e^{\zeta_t(h)}\right) \end{aligned} \tag{30}$$

Finally, combined (25), the matching model for FR can be described as follows:

$$max P_t(m) = \frac{e^{\zeta_t(m)}}{\sum_m^U e^{\zeta_t(m)}} \qquad \lambda_t(m) = 1 \tag{31}$$

where $\lambda_t(m) = 1$ indicates that SDGM at time $t$ match FR $m$.

Substituting (22) into (31), the FR with the highest probability is the optimal matching scheme according to the indicator variable about the feature information of multi-type FRs. Based on this, the matching of optimal FRs to SDGM is achieved in the initial matching round.

Specifically, the schematic of the complete matching process for multi-type FRs is as displayed in Fig. 4. Specifically, the optimal response powers of diversified FRs in matching round 1 are obtained within the day. Correspondingly, the regulated boundary of FRs and SDGM is updated as the known volume to be substituted into the next matching round. Following this, the matching sequence will be formed when the SDGM is 0 in matching round G.

The SDGM will be reduced by the certain response power of FR after the matching round $g$, then the feature matching in round $g+1$ will be performed. The SDGM in matching round $g$ is corrected to:

$$\begin{aligned} P_{SDGM}^{g+1}(t) &= P_{SDGM}^{g-1}(t) - P_m^g(t), g \geq 1 \\ P_{SDGM}^{0}(t) &= P_{SDGM}(t) \end{aligned} \tag{32}$$

where $Pg+1\ SDGM(t)$ and $Pg\text{-}1\ SDGM(t)$ are the power of the SDGM in matching round $g+1$ and $g$-1, respectively; $Pg\ m(t)$ is the power of FR $m$ in matching round $g$.

Continuing in this manner until the SDGM reaches 0 or the regulated boundaries of FRs are reached after matching round G. the stable set of response sequences for FRs is output, which can be expressed as:

$$[V]_{1*T} = [U]_{1*m}{}^{*}[\lambda]_{m*T} \tag{33}$$

where the corner scale of matrix is the number of matrix rows and columns; $[V]_{1*T}$ is the matrix of SDGM in period $T$; $[U]_{1*m}$ the matrix of FR in type $m$; $[\lambda]_{m*T}$ is the matching matrix of FR 0-$m$ and SDGM 0-$T$.

## III. Co-scheduling of Flexible Resources in Virtual Power Plant

This section elaborates on the structure of VPP optimal scheduling, including the acquisition, matching, and decomposition of SDGM. Furthermore, the multi-objective functions of the proposed method are transformed into a comprehensive cost function by quantifying the cost of FRs' response, willingness, and peak shaving. Additionally, equations and inequalities representing constraints are established, encompassing conventional resources, flexible loads (FLs), energy storage (ES), and peak shaving services.

### A. Framework for de-aggregation strategy

Building upon the feature matching described in Section II, this study

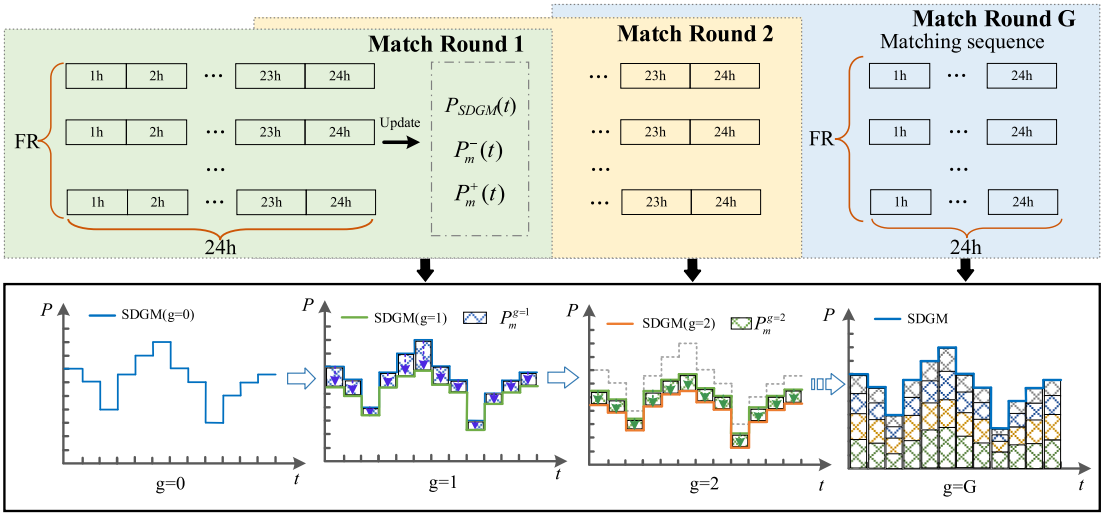


**Fig. 4.** Matching process of multi-type FRs.

concentrates on a collaborative response method employing feature matching for multi-type FRs to de-aggregate declared scheduled demand of VPP. The structure of proposed strategy is shown in Fig. 5.

(1) (1) The initial step involves establishing the co-scheduling scheme, which decomposes the total scheduled demand of the VPP and iteratively allocates it across the available multi-type FRs. The de-aggregation process not only aims to minimize the exchange power with the grid but also integrates two additional objectives: the willingness cost of the FRs and the peak shaving benefits for the VPP. These objectives ensure that resources with varying operational characteristics are optimally utilized. In this step, the total scheduled demand is iteratively decomposed, while respecting both the fundamental operational constraints of the VPP and additional factors such as peak shaving bidding capacity and actual output from FRs. This ensures that the VPP's scheduled demand is accurately met without exceeding resource limits. Further details of this step can be found in Section III (B).

(2) (2) The second step focuses on refining the heterogeneous features of the multi-type FRs and developing a generalized feature matching model to quantify the response willingness of each resource within the microgrid. This process begins by establishing a feature mapping framework, which translates the operational characteristics of the FRs into a format that can be compared against the VPP's scheduling command. Additionally, a discrete choice model is employed to facilitate the feature matching between the multi-type FRs and the scheduling command, ensuring that resources with the highest compatibility are prioritized. This matching is essential to maintain the internal power balance of the microgrid and optimize the PSAS offered by the VPP. The scheduling command is derived from the net load curve, which serves as the scheduled demand for the upcoming feature matching iteration. This detailed process is discussed further in Section II.

(3) (3) The co-scheduling of multi-type FRs and settlement of VPP are constructed in the third step. The de-aggregation strategy is implemented through a MILP optimization approach, which ensures that the scheduling command is effectively de-aggregated across the FRs while achieving both the power balance and peak shaving objectives. In this step, the response costs of the FRs and the peak shaving benefits of the VPP are calculated and evaluated, ensuring that the VPP operates optimally and efficiently while considering both technical and economic factors. This process, including the MILP formulation, is detailed in Section III.

It is worth noting that using the above-mentioned utility-maximizing criterion of discrete choice model, the peak shaving demand at each time are matched with the optimal FRs, determining both the types and response power of FRs required at each moment. Subsequently, in the following matching round, the adjustment boundary of FRs and peak shaving demand is updated based on the matching results from the previous round. This iterative process continues until either the adjustment boundary of FRs reaches 0 or the peak shaving demand is fulfilled. As a result, the sequence for FR matching is established within the G matching round.

B. De-aggregation strategy based on MILP

1) Objective functions

The diagram of improved de-aggregation strategy based on feature matching model is shown in Fig. 5. In comparison to the nonlinear optimization, the linearized MILP has a shorter computation time. Beyond that, MILP restricts some decision variables to integers, which is more appropriate for modeling match characteristics. Simultaneously, the real and integer decision variables enable MILP to model FR with greater flexibility.

In this work, the de-aggregation objective is to minimize the comprehensive costs of three aspects: response costs of multi-type FRs, peak shaving benefits of VPP, peak shaving benefits risk of VPP. The response cost of multi-type FRs consists of economy and willingness indicators. Besides, the economy is related to the cost feature, which is calculated as follows:

$$C_{FR} = \sum_t \sum_m c_m \rho_\omega |P_m(t)| \tag{34}$$

where $C_{FR}$ is the response cost of multi-type FRs.

The response willingness of multi-type FRs refers their response capability assessment and is related to potential and rate feature. The higher response capability, the higher the willingness. The response

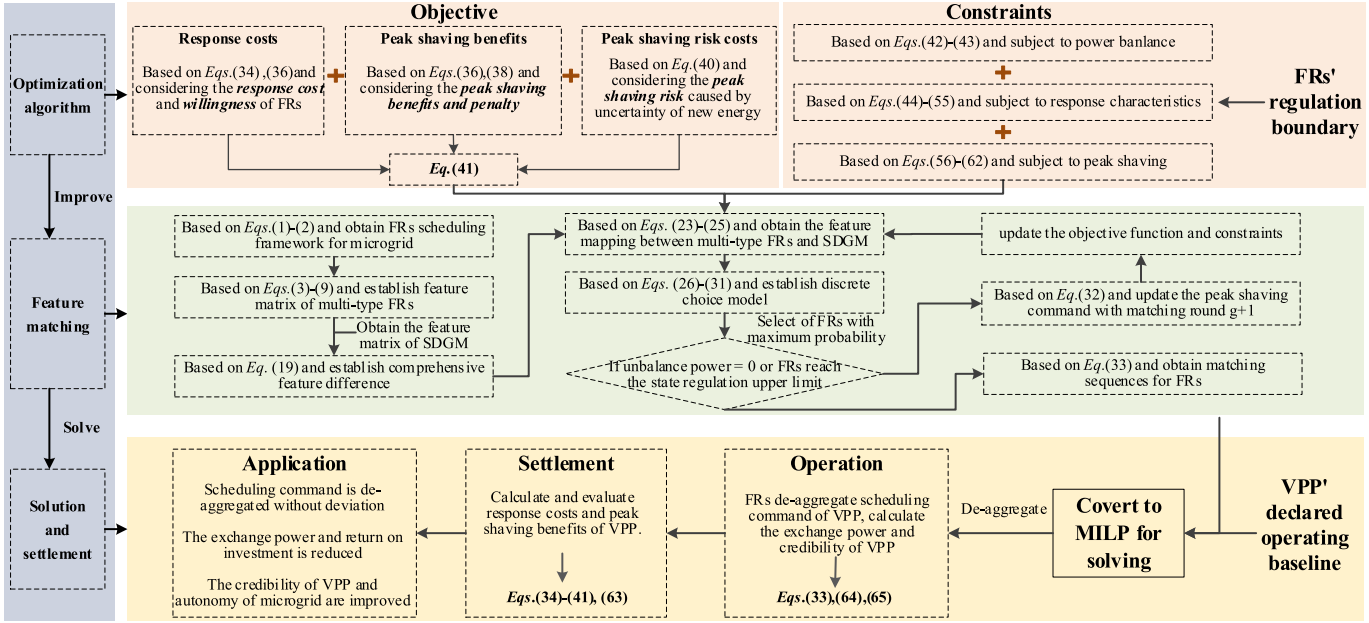


**Fig. 5.** Diagram of the MILP-based de-aggregation strategy.

willingness of multi-type FRs is translated into the economic indicators and expressed by:

$$C_{WL} = \sum_t c_{ca}\rho_\omega|E_m - E_t| + \sum_t c_{ra}\rho_\omega|R_m - R_t| + \sum_t c_{tm}\rho_\omega|L_m - L_t| + \sum_t c_{pt}\rho_\omega|Q_m - Q_t| \tag{35}$$

where $C_{WL}$ is the response willingness cost of FRs; $c_{ca}$, $c_{ra}$, $c_{tm}$, and $c_{pt}$ are the influenced coefficient of response willingness on the response potential, rate, time, and potential for multi-type FRs, respectively.

As the peak shaving strategy mentioned in Section II, the grid-connected microgrid participates in PSAS by reducing the power output of tie line and increasing the power input from main grid. Therefore, to enhance the initiative of PSAS, the certain benefits can be obtained from paid peak shaving [47], which can be calculated by:

$$B_{PS} = \sum_t b_{PS}\rho_\omega F_{PS}(t) \tag{36}$$

$$F_{PS}(t) = \begin{cases} P_{bid}(t) & P_{PS}(t) \geq P_{bid}(t) \\ P_{PS}(t) & \kappa P_{bid}(t) \leq P_{PS}(t) \leq P_{bid}(t) \\ 0 & P_{PS}(t) < \kappa P_{bid}(t) \end{cases} \tag{37}$$

where $B_{PS}$ is the peak shaving benefits of microgrid; $b_{PS}$ is compensation unit cost of VPP in peak shaving market; $F_{PS}(t)$ is peak shaving power; $P_{PS}(t)$ is the actual peak shaving output of VPP; $P_{bid}(t)$ is the day-ahead bidding capacity of VPP in peak shaving market at time $t$; $\kappa$ is the benchmark ratio of segmented peak shaving.

Meanwhile, the actual peak shaving output is assessed to ensure the responsiveness of VPP in participating in PSAS, and the peak shaving penalty cost can be calculated by:

$$C_{PP} = \sum_t c_{PP}\rho_\omega K_{PP}(t) \tag{38}$$

$$K_{PP}(t) = \begin{cases} 0 & P_{PS}(t) \geq \kappa P_{bid}(t) \\ P_{bid}(t) - P_{PS}(t) & P_{PS}(t) < \kappa P_{bid}(t) \end{cases} \tag{39}$$

where $C_{PP}$ is the peak shaving penalty cost of VPP; $c_{PP}$ is the unit penalty price of VPP in peak shaving market; $K_{PP}(t)$ is the assessed peak shaving power.

In the electricity market context, the bidding decisions for VPPs are challenging due to internal resource characteristics and market variability. This challenge arises primarily from the spatial and temporal nature of wind and PV, rendering the peak shaving strategy as a risk management issue in this paper [10]. Considering a discrete benefit distribution with a confidence $\alpha$, the CVaR is approximated as the expected loss for the set of a small probability 1-$\alpha$ scenario [48]. The CVaR can be expressed by:

$$\delta_{\mathrm{CVaR}} = \min_{\delta_{\mathrm{VaR}}, h_n} \delta_{\mathrm{VaR}} + \sum_n \rho_\omega h_\omega \Big/ (1-\alpha) \tag{40}$$

where $\delta_{\mathrm{VaR}}$ is the value of VaR; $\alpha$ is the pre-set confidence; $h_\omega$ is the introduced auxiliary variable, represents the difference between the peak shaving cost and $\delta_{\mathrm{VaR}}$.

The comprehensive costs are linearly weighted by above five indicators and expressed by:

$$obj = min(C_{FR} + C_{WL} - B_{PS} + C_{PP} + Y\delta_{\mathrm{VaR}}) \tag{41}$$

where $Y$ is the risk preference coefficient, indicates the preference degree of VPP for the peak shaving benefit risk. The larger the value of $Y$, the more conservative the peak shaving strategy adopted by VPP.

2) Constraints

The external characteristics of VPP is calculated by:

$$s.t. \begin{cases} P^g_{aec}(t) = P^g_{SDGM}(t) - P^g_{FL}(t) - P^g_{Wind}(t) - P^g_{PV}(t) \\ \qquad -P^g_{Gt}(t) - P^g_{Hy}(t) - P^g_{ES}(t) \\ P^g_{FL}(t) = \Delta P^g_{tr}(t) + \Delta P^g_{re}(t) + \Delta P^g_{ad}(t) \end{cases} \tag{42}$$

where $Pg\ aec(t)$ is the actual external characteristics of real-time operation for VPP in matching round $g$; $Pg\ Gt(t)$, $Pg\ Hy(t)$, $Pg\ Wind(t)$, and $Pg\ PV(t)$ is the output power of gas turbine, hydroelectric power unit, wind turbine, and PV in matching round $g$, respectively; $Pg\ ES(t)$ is the response power of ES in matching round $g$; $Pg\ FL(t)$ is the response power of FLs containing TLs, RLs, and ALs in matching round $g$; $\Delta Pg\ tr(t)$, $\Delta Pg\ re(t)$, and $\Delta Pg\ ad(t)$ are the response power of TLs, RLs, and ALs in matching round $g$, respectively.

The power balance constraint of VPP is characterized by:

$$P^g_{Gt}(t) + P^g_{Hy}(t) + P^g_{Wind}(t) + P^g_{PV}(t) + P^g_{ES}(t) = P^g_{ti}(t) + \Delta P^g_{tr}(t) + \Delta P^g_{re}(t) + \Delta P^g_{ad}(t) \tag{43}$$

where $Pg\ ti(t)$ is the tie-line power in matching $g$.

The constraints on new energy power of VPP are:

$$s.t. \begin{cases} P^{\min}_{Wind} \leq \sum_g P^g_{Wind}(t) \leq P^{fc}_{Wind} \\ P^{\min}_{PV} \leq \sum_g P^g_{PV}(t) \leq P^{fc}_{PV} \end{cases} \tag{44}$$

where $P\min\ wind$ is the minimum output of wind turbine; $P\min\ PV$ is the minimum output of PV.

The gas turbines can be regulated continuously by power range and ramp rate, which are as expressed by:

$$s.t. \begin{cases} \tau_{Gt}P^N_{Gt} \leq \sum_g P^g_{Gt}(t) \leq P^N_{Gt} \\ -R_{Gt} \leq P^g_{Gt}(t) - P^g_{Gt}(t-1) \leq R_{Gt} \end{cases} \tag{45}$$

where $\tau_{Gt}$ is the minimum output coefficient of gas turbine; $PN\ Gt$ is rated power of gas turbine; $R_{Gt}$ is the ramp limits gas turbine.

The hydroelectric power unit can be regulated continuously by power range and ramp rate, which are as follows:

$$s.t. \begin{cases} 0 \leq \sum_g P^g_{Hy}(t) \leq P^N_{Hy} \\ R^-_{Hy} \leq P^g_{Hy}(t) - P^g_{Hy}(t-1) \leq R^+_{Hy} \end{cases} \tag{46}$$

where $PN\ Hy$ is the rated power of hydroelectric power unit; $R\text{-}\ Hy$ and $R+\ Hy$ are the ramp limits for down and up regulation of hydroelectric power.

TLs denote the FLs that remain the total electricity consumption constant during the scheduled cycle, while electricity consumption with each time period can be adjusted flexibly within a certain range, typically represented by electric vehicles, disinfection cabinets, etc.

The constraint on response rate of FLs is:

$$v^- \leq dP^g_{FL}(t) \leq v^+ \tag{47}$$

where $v^-$ and $v^+$ are the rate limits for up and down regulation of FLs, respectively.

TLs are required to keep their electricity consumption constant during the dispatch cycle, which satisfy:

$$\sum_t^T \Delta P^g_{tr}(t) = 0 \tag{48}$$

The constraint on TLs response capacity is:

$$\alpha_{\min}P_{tr}(t) \leq \sum_g \Delta P^g_{tr}(t) \leq \alpha_{\max}P_{tr}(t) \tag{49}$$

where $\alpha_{\min}$ and $\alpha_{\max}$ are the response lower and upper limit coefficients for TLs; $P_{tr}(t)$ is the planned power consumption of the TLs at time $t$.

RLs refer to the FLs that can be partially or fully reduced for the loads

with low reliability requirements due to inadequate power supply, typically represented by air conditioning loads, water heaters, etc. The constraint on RLs response capacity is:

$$r_t \beta P_{re}(t) \le \sum_g \Delta P_{re}^g(t) \le P_{re}(t) \tag{50}$$

where $r_t$ is a 0–1 state variable characterizing the load reducible state at time $t$; $\beta$ is the response coefficient for RLs; $P_{re}(t)$ is the planned power consumption of the RLs at time $t$.

Constraint on the number of reduced regulation times for RLs is:

$$\sum_t^T r_t \le N_{\max} \tag{51}$$

where $N_{\max}$ is the upper number of reduced regulation times.

In addition to TLs and RLs, there are still other FLs characterized by adjustable power and high flexibility, which are summarized as ALs in this paper. The constraint on response capacity of ALs is:

$$\gamma_{\min} P_{ad}(t) \le \sum_g \Delta P_{ad}^g(t) \le \gamma_{\max} P_{ad}(t) \tag{52}$$

where $\gamma_{\min}$ and $\gamma_{\max}$ are the response lower and upper limit coefficients for ALs; $P_{ad}(t)$ is the planned power consumption of the ALs at time $t$.

The ES can be charged and discharged continuously within rated power range, which is expressed by:

$$s.t. \begin{cases} -P_{ES}^N \le \sum_g P_{ES}^g(t) \le P_{ES}^N \\ 0 \le E_S^0 + \sum_{t'} \sum_g \left[ P_{ES}^g(t') \Delta t \right] \le E_S^N, t' \in [0, t] \end{cases} \tag{53}$$

where *PN ES* is the rated power of ES; *E0 S* is the initial capacity of ES; *EN S* is the rated capacity of ES.

ES is constrained by constant energy at the beginning and end of scheduling, which is as follows:

$$\sum_t^T P_{ES}^g(t) = 0 \tag{54}$$

The constraints on response time of multi-type FRs is:

$$t_{m,min} \le t_{m,2} - t_{m,1} \le t_{m,max} \tag{55}$$

where $t_{m,\min}$ and $t_{m,\max}$ are the minimum and maximum response time of FR $m$.

The feature matching constraints of VPP are as follows (11) and (32).

The minimum bidding capacity constraint in the peak shaving market is as follows:

$$P_{bid,min} u(t) \le P_{bid}(t) \le M u(t) \tag{56}$$

where $P_{bid,\min}$ is the minimum bidding power in the peak shaving market; $u(t)$ is a 0–1 variable, indicates whether the VPP participates in the peak shaving market at time $t$.

The constrains of the actual peak shaving output are:

$$s.t. \begin{cases} 0 \le P_{PS}(t) \le \sum_g P_{aec}^g(t) - \sum_g P_{SDGM}^g(t) + (1 - u(t))M \\ P_{PS}(t) \le u(t) M \end{cases} \tag{57}$$

In this paper, the CVaR is used to quantify the impact caused by uncertainty of wind and PV output for peak shaving benefit. The peak shaving benefit and electricity curtailment of new energy is considered into peak shaving risk benefit. In order to facilitate the solution, the auxiliary variable $h_\omega$ in the CVaR model is relaxed as:

$$s.t. \begin{cases} \sum_t c_{cur} \left| \sum_g \left[ P_{Wind}^g(t) + P_{PV}^g(t) \right] \right| - B_{PS} - \delta_{\mathrm{VaR}} \le h_\omega \\ h_\omega \ge 0 \end{cases} \tag{58}$$

where $c_{cur}$ is the unit cost of wind and PV curtailment. Additionally, due to (58) is expressed as the peak shaving cost, the peak shaving risk benefit is negative for $\delta_{CVaR}$.

Introducing an auxiliary variable $P_{new}(t)$, the (58) is linearized as:

$$s.t. \begin{cases} \sum_t c_{cur} P_{new}(t) - B_{PS} - \delta_{\mathrm{VaR}} \le h_\omega \\ h_\omega \ge 0 \\ P_{new}(t) \ge \sum_g \left[ P_{Wind}^g(t) + P_{PV}^g(t) \right] \\ P_{new}(t) \ge -\sum_g \left[ P_{Wind}^g(t) + P_{PV}^g(t) \right] \end{cases} \tag{59}$$

where $P_{new}(t)$ is the introduced auxiliary variable.

Similarly, considering the nonlinearization of absolute value in (34) and (35), which are linearized as:

$$C_{FR} = \sum_t \sum_m c_m \rho_\omega P_{FR}$$
$$\begin{cases} P_{FR} \ge P_m(t) \\ P_{FR} \ge -P_m(t) \end{cases} \tag{60}$$

$$C_{WL} = \sum_t c_{ca} \rho_\omega E_{ca} + \sum_t c_{ra} \rho_\omega R_{ra} + \sum_t c_{tm} \rho_\omega L_{tm} + \sum_t c_{pt} \rho_\omega Q_{pt}$$
$$\begin{cases} E_{ca} \ge E_m - E_t, E_{ca} \ge -(E_m - E_t) \\ R_{ra} \ge R_m - R_t, R_{ra} \ge -(R_m - R_t) \\ L_{tm} \ge L_m - L_t, L_{tm} \ge -(L_m - L_t) \\ Q_{pt} \ge Q_m - Q_t, Q_{pt} \ge -(Q_m - Q_t) \end{cases} \tag{61}$$

where $P_{FR}$, $E_{ca}$, $R_{ra}$, $L_{tm}$ and $Q_{pt}$ are the introduced auxiliary variables.

Considering the nonlinearity and difficulty in solving the piecewise function in (36)–(39), linearize them as:

$$\begin{cases} 0 \le F_{PS}(t) \le P_{bid}(t) \\ F_{PS}(t) \le P_{PS}(t) \\ P_{PS}(t) - \kappa P_{bid}(t) \ge (a_{\omega t} - 1) M \\ P_{PS}(t) - \kappa P_{bid}(t) \le (1 - b_{\omega t}) M \\ a_{\omega t} + b_{\omega t} = 1 \\ F_{PS}(t) \le a_{\omega t} M \\ K_{PP}(t) \ge P_{bid}(t) - P_{PS}(t) + (b_{\omega t} - 1) M \\ K_{PP}(t) \ge 0 \end{cases} \tag{62}$$

where $a_{\omega t}$, $b_{\omega t}$ are the introduced 0–1 state variables.

To analyze the effect of the de-aggregation strategy, the economic benefit of multi-type FRs is calculated by (34). Moreover, to assess the economic cost of scheduled demand consumption on VPP, the return on investment of de-aggregation is calculated by:

$$B_{UC} = C_{FR} \Big/ \sum_t \sum_m P_m(t) \Delta t \tag{63}$$

where $B_{UC}$ is the return on investment of de-aggregation.

The VPP is generally equipped with a limited aggregated and stochastic capacity, and should ensure that it declares the credible regulation capacity for different system regulation requirements [10]. Therefore, to evaluate the credibility of VPP participating in PSAS, the peak shaving benefit and deviation penalty can be derived as (36) and (38).

$$Cr_{PS} = \left( \sum_t P_{PS}(t) \Delta t \Big/ \sum_t P_{bid}(t) \Delta t \right) \times 100\% \tag{64}$$

where $Cr_{PS}$ is the credibility of VPP participating in PSAS.

To assess the exchange power through tie-line between microgrid and main grid, the autonomy of microgrid is defined as:

$$Au_{Mg} = 1 - \frac{\sum_t \sum_g P_{ti}^g(t) \cdot \Delta t}{\sum_t P_{ti}^{\max} \cdot \Delta t} \tag{65}$$

where $Au_{Mg}$ is the autonomy of microgrid; $P\max\ ti$ is the rated power of

tie-line between microgrid and the main grid.

C. Summary of the de-aggregation strategy based on MILP

Based on the linearization process, the de-aggregation strategy can be converted into a MILP model mathematically expressed as (63). This MILP model can be effectively solved by employing commercial solvers such as Gurobi.

$$\underset{\mathrm{C,B}}{objmin}(41)$$
$$s.t.(11),(32),(42)-(62)$$
$$\mathrm{C}=\left\{P^{g}_{Gt,i}(t),P^{g}_{Hy}(t),P^{g}_{Wind}(t),P^{g}_{PV}(t),P^{g}_{ES}(t),P^{g}_{ti}(t),\Delta P^{g}_{tr}(t),\Delta P^{g}_{re}(t),\Delta P^{g}_{ad}(t),t_{m,2},t_{m,1},r_t,P^{g}_{bid}(t),P^{g}_{SDGM}(t),P_{PS}(t)\right\} \quad (66)$$
$$\mathrm{B}=\{\lambda_t(m),r_t,u(t),a_{\omega t},b_{\omega t}\}$$

where **C** and **B** are the set of continuous and binary variables, respectively.

IV. Cases Study

In this section, case studies are conducted to validate our proposed method. The studied comparative cases are firstly introduced. Subsequently, the results and relevant discussions concerning FRs response, feature matching, peak shaving and economic benefits, are further presented.

A. Case descriptions

To demonstrate the feasibility and effectiveness of the proposed feature matching method, the MILP based power balance regulation and de-aggregation strategy are run on MATLAB 2021. The configuration of actual microgrid in western China is shown in Fig. 6, and the details of tested microgrid are displayed in Table 2. The schematic of VPP's declared peak shaving plan is shown in Fig. 7. Several different cases are conducted by considering feature matching characteristics of FRs and PSAS for the main grid, which are as follows. And the cases comparison is as shown in Table 3.

Case 1: Power balance of microgrid is simulated without FRs regulation. Fig. 6 illustrates the declared baseline for VPP.

Case 2: the scheduling command of VPP is de-aggregated to FRs but ignores feature matching and PSAS.

Case 3: the scheduling command of VPP is de-aggregated to FRs considering PSAS but ignores feature matching.

Case 4: the scheduling command of VPP is de-aggregated to FRs considering source-load matching but ignores PSAS.

Case 5: the scheduling command of VPP is de-aggregated to FRs considering source-load matching and PSAS.

**Table 2**
Technical parameters of the regional microgrid.

| Type | Rated power/ MW | Minimum power/ MW | Configurated quantity |
|---|---|---|---|
| Gas turbine | 5 | 2.5 | 1 |
| PV | 17.64 | 0 | 5 |
| Wind turbine | 44.6 | 0 | 4 |
| Hydroelectric power unit | 33 | 0 | 1 |
| Tie-line | 15 | −15 | – |
| Industrial loads | 111.08 | – | – |
| Transferable loads | 58.46 | $0.7*P_{tr}(t)$ | – |
| Reducible loads | 29.84 | $0.7*P_{re}(t)$ | – |
| Adjustable loads | 10.79 | $0.7*P_{ad}(t)$ | – |
| Energy storage | 20 | −20 | 3 |

Case 6: the scheduling command of VPP is de-aggregated to FRs considering feature matching but ignores PSAS.

Case 7: the scheduling command of VPP is de-aggregated to FRs considering the proposed strategy with feature matching and PSAS.

B. VPP de-aggregation analysis using feature matching

In this paper, the declared operating baseline of VPP as depicted in Fig. 7, is treated as the scheduling command containing internal power demand and PSAS for the main grid. The optimal response sequence of multi-type FRs within microgrid is achieved by the proposed de-aggregation strategy for VPP, ensuring that the scheduling command is satisfied to maintain power balance within the microgrid. Nevertheless, the de-aggregation of VPP encounters difficulties in assessing exchange power due to insufficient consideration of the heterogeneity of multi-type FRs. As a result, the microgrid may struggle to precisely respond to the scheduling command and subsequently participate in PSAS due to the lack of VPP' credibility.

The comparison of case 2, case 4 and case 6 highlights that the feature matching method's effectiveness in minimizing exchange power and improving comprehensive benefits when peak shaving conditions are ignored. Similarly, the comparison of case 3, case 5 and case 7 demonstrates the effectiveness of the proposed de-aggregation strategy in enhancing comprehensive benefits and participating in PSAS. Fig. 8 illustrates the response sequence by multi-type FRs from case 2 to case 7 on a typical day. The exchange power between the microgrid and main grid through tie-line directly reflect the internal power imbalance. Specifically, the causes of exchange power in case 2 and 4 are compared with case 6 and analyzed in detail. The exchange power in case 2 and 4 are 247.52MWh and 240.83MWh, respectively, for the day. In case 2, the de-aggregation of VPP does not consider the source-load matching, resulting in a delay in tracking loads and generation to reduce the

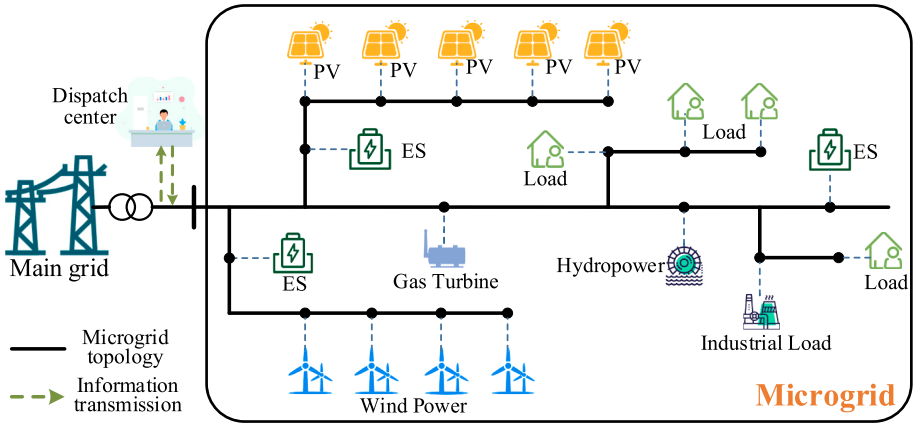


**Fig. 6.** Configuration of a microgrid system in western China.

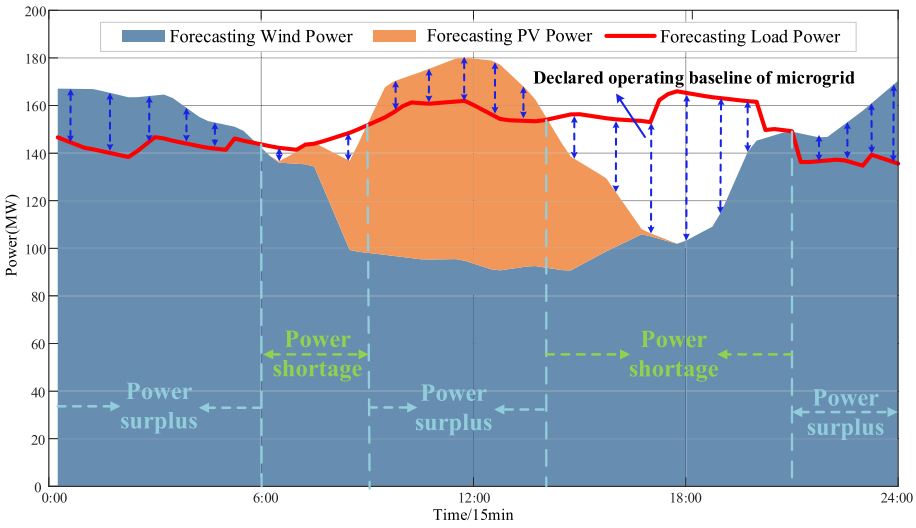


**Fig. 7.** Schematic of the declared operating baseline for VPP.

**Table 3**
Conducted cases comparison.

| Case | Feature matching methods | PSAS | The scheduling command de-aggregating |
|---|---|---|---|
| Case 1 | ×[1] | × | × |
| Case 2 | × | × | ✓[2] |
| Case 3 | × | ✓ | ✓ |
| Case 4 | Source-load matching | × | ✓ |
| Case 5 | Source-load matching | ✓ | ✓ |
| Case 6 | Proposed feature matching | × | ✓ |
| Case 7 | Proposed feature matching | ✓ | ✓ |

1 × indicates that the content is not being considered.
2 ✓ indicates that the content is considered

imbalanced power of the microgrid. It is important to note that the source-load matching is established by analogy with eqs. (5) and (19), considering only the change direction and power imbalance of generation and load. With the proposed feature matching method in case 6, the exchange power is reduced to 104.65MWh for the day. This reduction is attributed to the feature matching, which effectively enhance feature information interaction between power demand and supply, and fully leveraging the complementary scheduling potential of multi-type FRs in the microgrid.

In addition, the wind and PV curtailment resulting from power surplus of microgrid amounts to 585.26MWh in case 4, representing a 1.33 % increase compared to case 2. This increase can be attributed to the consideration of the power change direction of generation and load at next moment in the source-load matching model, which neglects the complementary characteristics and feature heterogeneity of multi-type FRs in microgrid. Addressing this drawback, the electricity curtailment in case 6 is reduced by 52.47 % compared to case 4, thanks to the proposed de-aggregation strategy considering feature matching. From Fig. 8, it is observed that the gas turbine maintains almost the minimum technical output across case 2 to case 7 due to its smaller installed capacity and higher carbon emission penalty cost. Meanwhile, it is noteworthy that the response power of ES in case 6 is 535.63MWh for the day, representing improvements of 6.79 % and 11.69 % compared to case 2 and case 4, respectively.

This enhanced response can be attributed to feature matching and excellent characteristics of ES, containing its response rate, response time, and response potential. These attributes allow the ES to avoid the limitations associated with being solely dependent on a single feature as the scheduling criterion, such as high response cost. In a word, the de-aggregation strategy considering feature matching plays a significant role in promoting utilization of ES, reducing exchange power, and mitigating electricity curtailment within the microgrid.

The response costs analysis of the multi-type FRs are recorded in Table 4, aiming to verify whether feature matching is considered in the de-aggregation strategy for the cost of exchange power, electricity curtailment, and FRs response, respectively. The comparison situation of exchange power cost, electricity curtailment cost, and ES cost aligns with previous technical analysis in case 2, 4, and 6. In case 2, only the response cost of multi-type FRs for economic scheduling decomposition is considered, as depicted in eq. (34), resulting in significantly lower FRs cost compared to case 4 and case 6. However, with the inclusion of source-load matching, the additional penalty cost of source-load deviation contributes to the increased FRs cost. Similarly, the response willingness cost of multi-type FRs, caused by feature differences, is one of the main reasons for the increased FRs cost in case 6.

Compared to VPP de-aggregation strategy that do not consider feature matching, the response sequence of multi-type FRs with feature matching can reduce internal imbalanced power and electricity curtailment, but increase the FRs cost. This increase in cost is attributed to the fact that the FRs matched by the proposed probability discrete choice model represent the optimal response based on the extracted feature structure. This refinement and iteration of the VPP de-aggregation process effectively satisfy the SDGM. However, exchange power and FRs cost reflect the ability and cost of optimal operation for microgrid from different perspectives, making it difficult to uniformly quantify the relationship between VPP de-aggregation and FRs cost and assess the economic cost of scheduled demand consumption on VPP. Consequently, the return on investment of de-aggregation is defined to characterize economic cost of decomposing unit power for scheduled demand, as shown in eq. (63). As observed from Table 4, although case 6 has the highest FRs cost, the return on investment of de-aggregation is the lowest. Alternatively, the economic cost of case 6 is lower when decomposing the same scheduled demand. Thus, the proposed de-aggregation strategy considering feature matching can effectively and economically decompose scheduling command.

As describe previously in Section II, this paper analyzes response characteristics to refine various types of generalized feature and construct the feature matching method to leverage regulated potential of multi-type FRs to participate in VPP de-aggregation. Fig. 9 depicts the comprehensive matching degree of multi-type FRs in the Logit model mentioned in Section II. The comprehensive matching degree is composed of the initial matching degree and the random perturbed

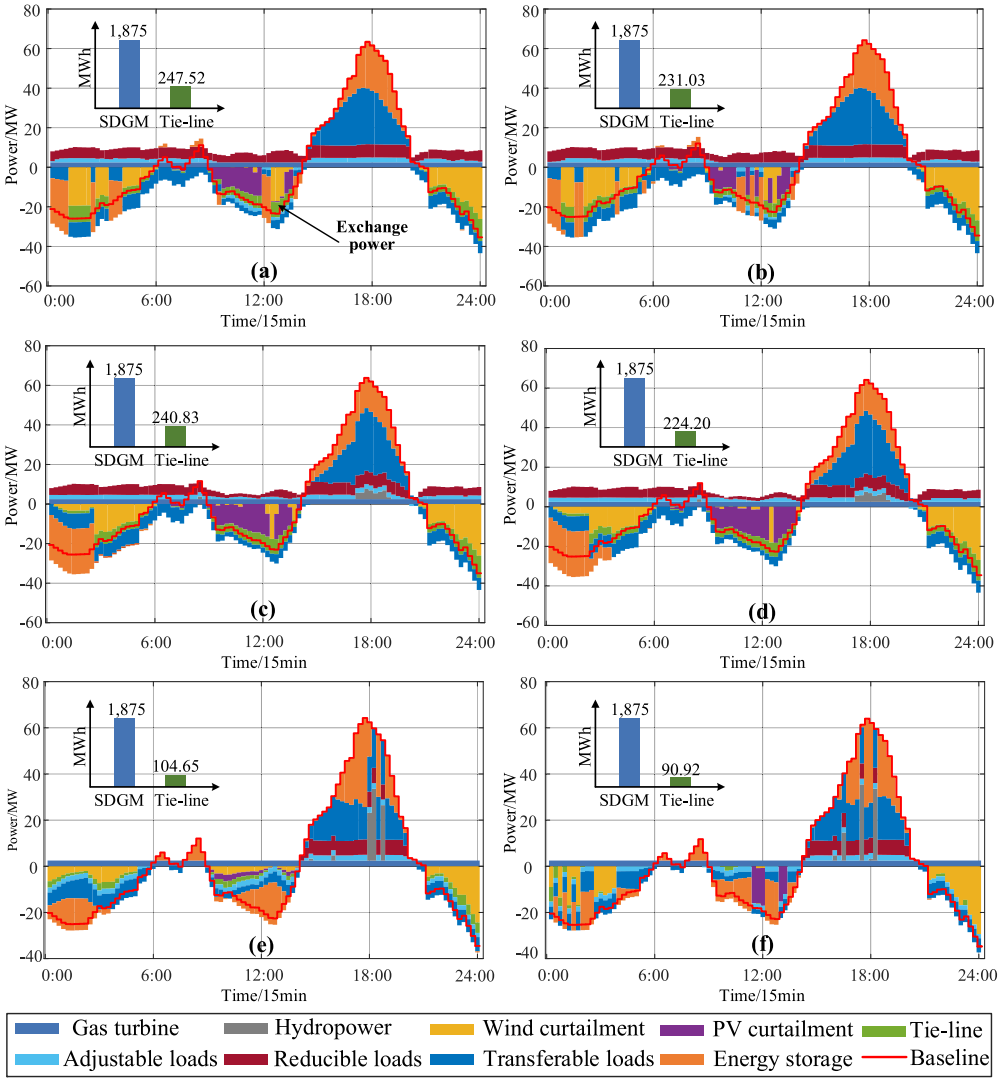


**Fig. 8.** Response sequence of multi-type FRs within microgrid in case 2 to 7: a) response sequence of multi-type FRs in case 2; b) response sequence of multi-type FRs in case 3; c) response sequence of multi-type in case 4; d) response sequence of multi-type FRs in case 5; e) response sequence of multi-type FRs in case 6; f) response sequence of multi-type FRs in case 7.

**Table 4**
Partial response cost of multi-type FRs in case 2–7.

| Case | Exchange power cost/$ | Electricity curtailment cost/$ | ES cost/$ | FRs cost/$ | Return on investment/$ |
|---|---|---|---|---|---|
| Case 2 | 13,861 | 40,429 | 12,625 | 157,946 | 97.0 |
| Case 3 | 12,937 | 41,584 | 12,632 | 160,205 | 97.5 |
| Case 4 | 13,046 | 40,968 | 12,070 | 159,782 | 98.3 |
| Case 5 | 11,815 | 42,156 | 12,118 | 162,026 | 98.7 |
| Case 6 | 5860 | 19,462 | 13,489 | 163,646 | 93.9 |
| Case 7 | 5091 | 18,223 | 13,511 | 165,116 | 92.5 |

term. Among them, the initial matching degree is related to the proposed response capacity, response rate, response time, response potential and response cost of the FRs. The extreme value distribution of the random perturbed term can be used to transform the comprehensive matching degree into a decision criterion only related to the initial matching degree. In a word, the smaller the difference between the response capacity, response rate, response time, response potential, response cost and peak shaving demand characteristics of the FR, the higher the comprehensive matching degree. Therefore, the utility maximization criterion based on the maximum comprehensive matching degree in the discrete selection model can achieve the matching priority.

Additionally, Fig. 10 illustrates the feature matching relationship between multi-type FRs and SDGM in case 6 and 7, providing detailed matching information for each unit hour to illustrate key matching information. As a note, the Gt, Hy, Wd, and Ti in Fig. 9 and 10 represent gas turbine, hydroelectric power unit, wind turbine, and tie-line, respectively. It can be observed that the capacity of SDGM is 1875MWh for the day, as shown in Fig. 7, and the scheduled demand is highest between 16:00 to 22:00, as shown in Fig. 9. During the scheduling period, the ES with higher response capacity, response potential, and response rate is prioritized to match SDGM in case 6, as verified in Fig. 9 and 10. And due to the low cost of electricity regulation as displayed in eqs. (34) and (35), the TLs also have a certain priority in VPP de-aggregation. Conversely, response capacity and response potential are no longer the main feature factors for FRs matching when SDGM is lower. Taking scheduling period 10:00–14:00 as an example to illustrate, the hydroelectric power with low response capacity is prioritized

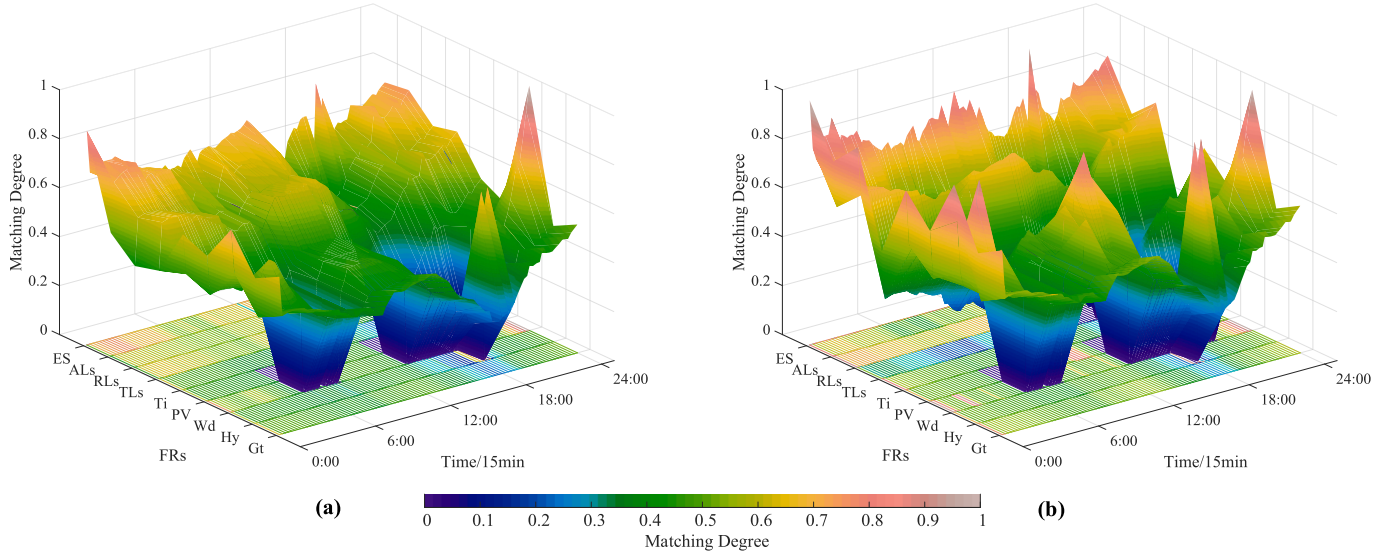


**Fig. 9.** Comprehensive matching degree for multi-type FRs in case 6 and 7: a) Matching degree in case 6; b) Matching degree in case 7.

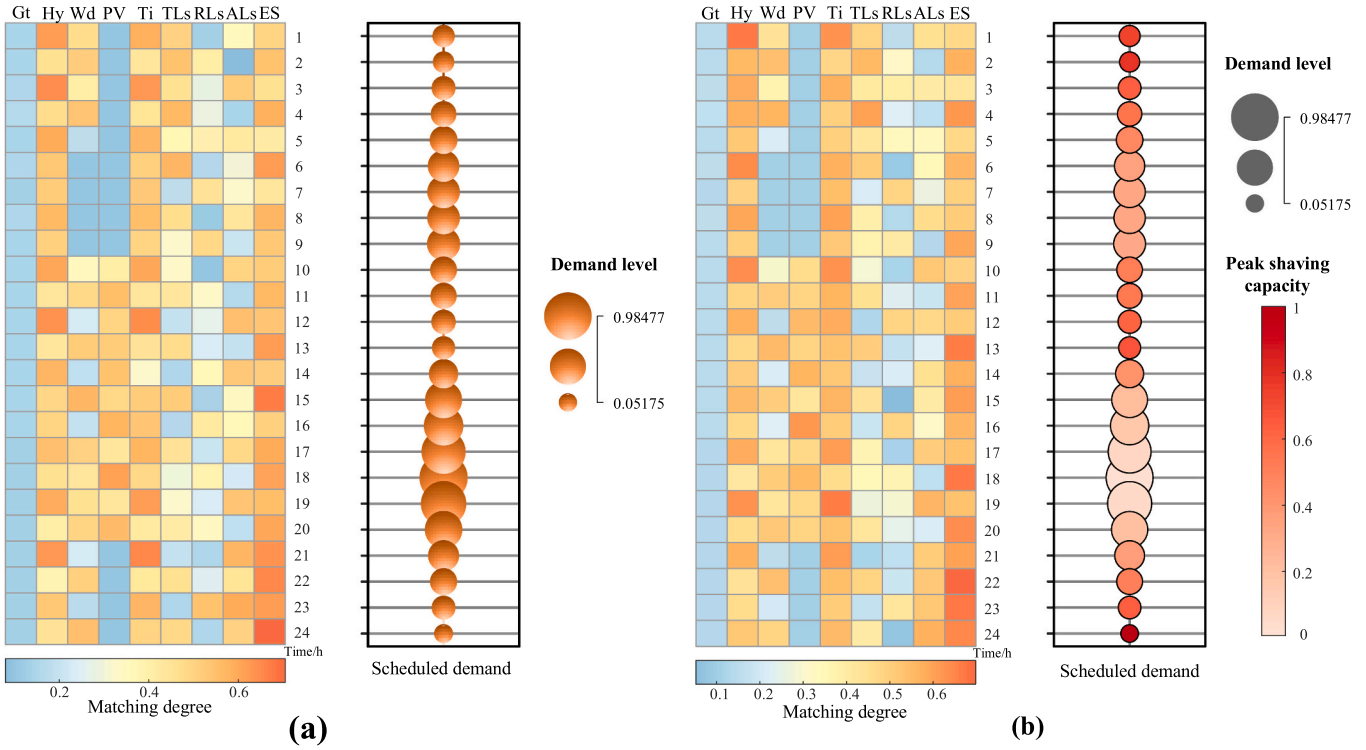


**Fig. 10.** Feature matching between multi-type FRs and scheduled demand in case 6 and 7: a) Feature matching between multi-type FRs and scheduled demand in case 6; b) Feature matching between multi-type FRs and scheduled demand in case 7.

to decompose the scheduled demand. It is concluded that the proposed feature matching method can effectively share the feature information between multi-type FRs and SDGM, and coordinating power demand and supply to leverage complementary scheduling potential.

### C. VPP de-aggregation analysis using PSAS

The declared baseline of VPP comprises day-ahead forecasted net load curves, ensuring fairness in the peak shaving market, as depicted in Fig. 8. Ulteriorly, the actual peak shaving output is determined by the difference between the declared baseline and the actual operating curve. In this paper, the benchmark ratio of segmented peak shaving, set at 70 %, is employed to assess the actual peak shaving output [49,50], its sensitivity analysis will be subsequently carried out. This ratio aims to mitigate peak shaving profit risks by reducing bidding capacity. In essence, if the actual peak shaving output of VPP falls below the bidding capacity and the deviation exceeds 30 %, the peaking benefits will not be settled, and VPP will incur deviation penalties. Conversely, if the actual peak shaving output of VPP exceeds the bidding capacity, the peak shaving benefits for the period will be settled according to the bidding capacity, as outlined in eqs. (37) and (39). Meanwhile, given that the peak shaving market settles only up to the bidding capacity, VPP will be incentivized to increase its bidding capacity for higher profits.

The response sequence of case 3, 5, and 7 considering PSAS, are

depicted in Fig. 8 (b), (d), and (e), respectively, utilizing economic dispatching, source-load matching, and feature matching, respectively. As described previously in Section II, the transmission power of tie lie is taken as the assessment basis for VPP participating PSAS. The exchange power in case 3 and 5 amounts to 231.03MWh and 234.2MWh, respectively, while the case 7 with feature matching is reduced by 60.6 % and 61.17 % compared with case 3 and 5. This reduction is attributed to the feature matching, which enhances the complementary capability of multi-type FRs promoting PSAS participation and reducing exchange power. Meanwhile, the electricity curtailment and ES response capacity of case 7 are 260.33MWh and 536.16MWh, respectively, which are superior to case 3 and 5. In summary, the effectiveness and superiority of proposed feature matching method have also been verified when considering VPP participation in PSAS, consistent with the previous analysis in Section IV (B). Additionally, Fig. 9 and 10 depict comprehensive matching degree and feature matching between multi-type FRs with SDGM in case 6 and 7. The comprehensive matching degree in case 7 exhibits a more pronounced trend compared to case 6 from Fig. 9. The main reason is that the benefits of VPP participating in PSAS can stimulate the response capability of multi-type FRs to reduce the comprehensive cost of VPP. In Fig. 10 (b), the heat map displays the matching degree of case 7 between multi-type FRs and SDGM for the day, while the bubble chart represents the scheduled demand in the day, with bubble size and shades reveal demand level and peak shaving capability of VPP participation, respectively. As can be seen that the higher the scheduled demand level, the smaller peak shaving capability. This is because the higher scheduled demand, caused by net load, requires more FRs regulation to maintain the power balance of the microgrid.

Furthermore, the actual peak shaving output of VPP comprises the sum of FLs adjusted power, ES charging power, and adjusted power of power supply, as shown in Fig. 8. Based on the proposed peak shaving strategy, Fig. 11 (a), (b) and (c) illustrate the day-ahead bidding capacity and actual peak shaving output of VPP, with maximum peak shaving deviations are 9.71 MW, 6.18 MW, and 5.93 MW in case 3, 5 and 7, respectively. The peak shaving deviation of case 7 amounts to 8.6MWh for the day, representing reductions of 70 % and 48.8 % compared to case 3 and 5, respectively. This reduction can be attributed to the proposed feature matching method, which contributes to reducing peak shaving deviation, improving de-aggregation of VPP. Meanwhile, Table 5 provides comprehensive assessments of VPP participating in PSAS. Specifically, the peak bidding capacity of case 7 is 932.7MWh, reduced by 1.83 % and 0.91 % compared to case 3 and 5, respectively. However, the actual peak shaving output of case 7 is 924.1MWh, closed to case 6, and increased by 2.7 MW compared with case 3. Notably, the credibility of VPP has been enhanced from 96.9 % to 99.1 % through the proposed feature matching method. It is concluded that the proposed de-aggregation strategy improves capability of VPP participating in PSAS and enhances credibility of VPP.

The comprehensive cost analysis of case 3, 5, and 7 considering PSAS is presented in Fig. 12. The peak shaving benefit, risk cost and penalty cost are consistent with the aforementioned technical analysis. Combined with eq. (41), the comprehensive costs of VPP amount to $117,451 in case 7, representing increases of $1489 and $2247 compared to case 3 and 5, respectively. This increase is primarily attributed to feature matching, which coordinates diversified features, not limited to cost features. Likewise, the return on investment mentioned in eq. (63) characterizes the economic cost of decomposing unit power for scheduled demand. The return on investment of de-aggregation of case 7 is $65.83/MWh, which reduced by 6.05 % and 6.9 % compared with case 3 and 5, respectively. Additionally, considering (65), the autonomy of microgrid in case 7 are elevated by 37.02 % and 3.82 % compared with case 5 and 6, respectively. Furthermore, the

**Table 5**
Comprehensive assessments of VPP participating in PSAS.

| Case | Bidding capacity/ MWh | Actual peak shaving output/ MWh | Autonomy of microgrid | Credibility of VPP |
|---|---|---|---|---|
| Case 3 | 950.1 | 921.4 | 35.83 % | 96.9 % |
| Case 5 | 941.3 | 924.5 | 37.72 % | 98.2 % |
| Case 7 | 932.7 | 924.1 | 74.74 % | 99.1 % |

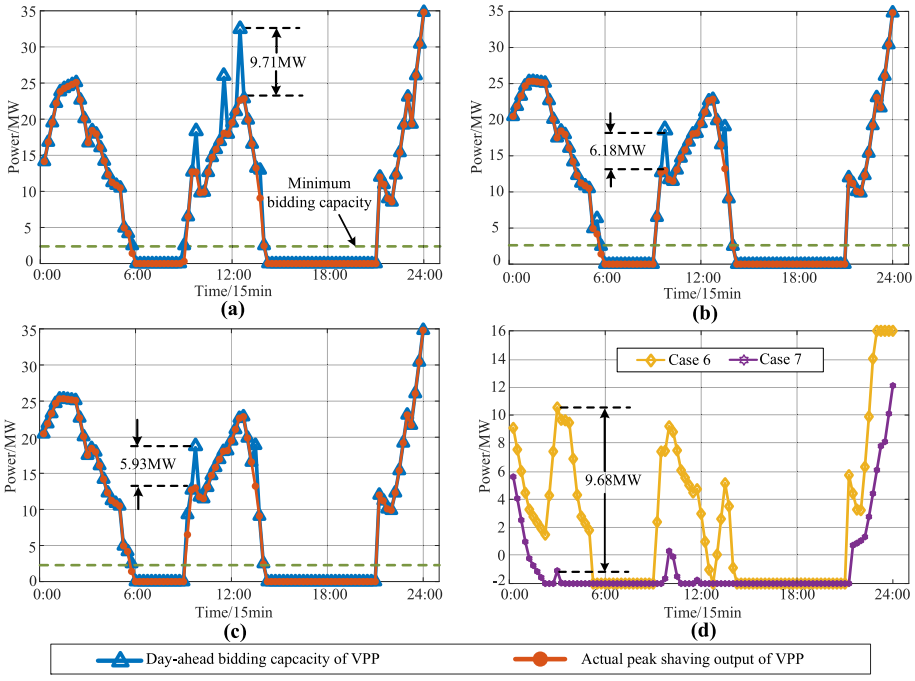


**Fig. 11.** Peak shaving power and tie-line power of VPP: a) peak shaving power of VPP in case 3; b) peak shaving power of VPP in case 5; c) peak shaving power of VPP in case 7; d) tie-line power of VPP in case 6 and 7.

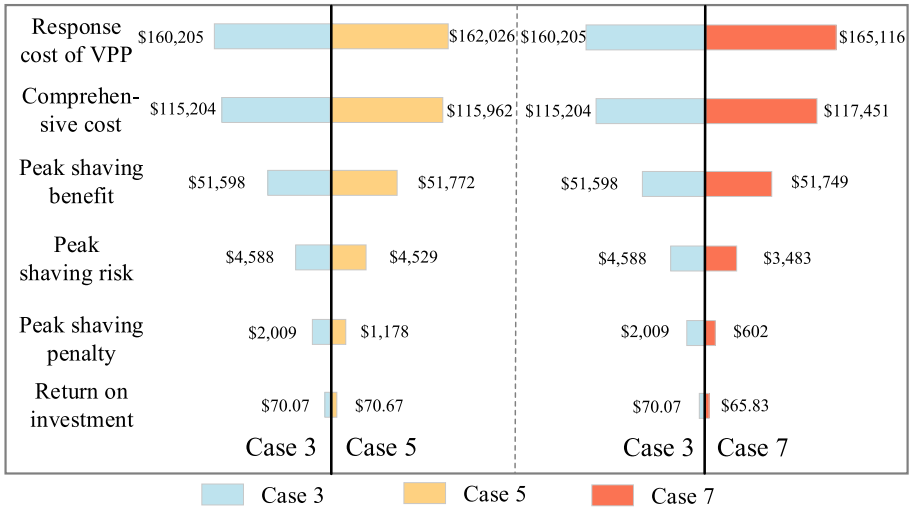


**Fig. 12.** Comprehensive cost analysis of VPP in case 3, 5, and 7.

maximum exchange power of case 7 is reduced by 9.68 MW compared with case 6. These results fully illustrate the proposed co-scheduling method can promote the autonomy of the microgrid, and reduce the frequent power exchange between microgrid and main grid.

Finally, sensitivity analysis was conducted on the benchmark values for segmented peak shaving, as shown in the Table 6. It's evident that as the benchmark value for peak shaving increases, the peak shaving benefits of the VPP decrease, while the comprehensive operating cost rises. Consequently, to mitigate the risk stemming from incomplete peak shaving tasks, the total bidding capacity of the VPP has been reduced. In essence, as the benchmark value for peak shaving increases, the assessment of the VPP by the peak shaving market becomes more rigorous.

To effectively compare the effectiveness of the proposed strategy, the technical and economic benefits of existing related research are summarized in Table 7. The comparative analysis highlights the significant advantages of the proposed VPP de-aggregation strategy using feature matching, which demonstrates enhanced capabilities in reducing return on investment and improving the autonomy of microgrids. These results validate the efficacy of our approach in optimizing VPP operations, particularly for applications requiring both economic and operational improvements.

## V. Conclusion

This paper proposes a de-aggregation strategy of VPP to collaboratively schedule multi-type FRs, considering feature matching and peak shaving services. Given the heterogeneous features of multi-type FRs, feature matching method and de-aggregation strategy are studied to optimize the comprehensive costs of the VPP. The peak shaving trading mechanism participated by VPP is investigated using bidding and virtual external characteristics model. The results indicate that:

1) The proposed generalization feature modeling has demonstrated its effectiveness in eliminating feature heterogeneity and achieving feature difference quantification. Additionally, the establishment of feature mapping and discrete choice models aids in deconstructing the decision-making process for response priority and feature matching.
2) The dynamic response sequences of multi-type FRs corresponding to scheduled demand in each matching round are formulated, which contributes to enhance the autonomy of microgrid and complementary response capability of multi-type FRs, while reducing the exchange power and electricity curtailment by 13.1 % and 53.8 %, respectively.
3) The response coupling relationship between power balance demand and peak shaving is clarified and modeled, meanwhile the peak shaving mechanism of VPP is developed considering the bidding capacity and actual external characteristics to improve the credibility of VPP and the return on investment by 2.2 % and 6.1 %, respectively.

Regarding future work, the proposed strategy will be extended to verify the feasibility of incorporating feature matching and peak shaving among multi-microgrids. Additionally, we will concentrate on reducing the response cost of FRs and developing the de-aggregation strategy for optimally co-scheduling multi-type FRs in auxiliary service market, while taking into account additional features of FRs. Furthermore, the feature matching method can be implemented to hierarchical scheduling of multiple power grids, such as urban-level, county-level, park-level grid, etc.

**Table 6**
The sensitivity analysis for benchmark ratio of segmented peak shaving.

| Benchmark ratio of segmented peak shaving | Comprehensive cost/$ | Peak shaving benefit/$ | Bidding capacity/MWh |
|---|---|---|---|
| 0.7 | 117,451 | 51,749 | 932.7 |
| 0.8 | 120,451 | 51,383 | 875.7 |
| 0.9 | 122,545 | 50,668 | 765.6 |

**Table 7**
The technical and economic benefits comparison between proposed strategy and related studies.

| Reference | System characteristics | Cost saving (%) | Power saving (%) | Key advantage |
|---|---|---|---|---|
| [51] | VPP interconnecting microgrid | 7.09 % | Not Applicable | Reducing total net present cost |
| [52] | VPP with microgrid by binary backtracking search algorithm | 10–15 % | About 4 % | Reducing total cost and exchange power |
| [53] | VPP with ES degradation | 7.7 % | Not Applicable | Reducing optimal revenue |
| Our work | VPP de-aggregated by feature matching | 6.1 % | 13.1 % | Reducing return on investment and exchange power |

## CRediT authorship contribution statement

**Zixuan Zheng:** Writing – review & editing, Writing – original draft, Visualization, Supervision, Software, Project administration, Methodology, Investigation, Formal analysis, Data curation, Conceptualization. **Jie Li:** Writing – review & editing, Writing – original draft, Software, Resources, Methodology, Formal analysis, Data curation, Conceptualization. **Xiaoming Liu:** Writing – original draft, Supervision, Resources, Methodology, Formal analysis, Data curation. **Chunjun Huang:** Visualization, Validation, Supervision, Methodology. **Wenxi Hu:** Writing – review & editing, Visualization, Supervision, Methodology, Data curation. **Xianyong Xiao:** Visualization, Validation, Supervision, Resources, Methodology. **Shu Zhang:** Writing – original draft, Resources, Formal analysis, Data curation. **Yongjun Zhou:** Supervision, Methodology, Funding acquisition, Data curation. **Song Yue:** Visualization, Supervision, Resources, Funding acquisition. **Yi Zong:** Visualization, Validation, Supervision.

## Declaration of competing interest

The authors declare that they have no known competing financial interests or personal relationships that could have appeared to influence the work reported in this paper.

## Acknowledgments

This work is supported by the Science and Technology Major Project of Tibetan Autonomous Region of China [Grant No. XZ202201ZD0003G].

## Data availability

Data will be made available on request.

## References

[1] Jiang B, Raza MY. Research on China's renewable energy policies under the dual carbon goals: A political discourse analysis. Energy Strateg Rev 2023;48:101118. https://doi.org/10.1016/j.esr.2023.101118.
[2] Silva G-S, Miguel H, Salman M, Goncalo C, Robin G, George K. A stochastic optimal power flow for scheduling flexible resources in microgrids operation. Appl Energy 2018;229:201–8. https://doi.org/10.1016/j.apenergy.2018.07.114.
[3] Xue Y, Li Z, Lin C, Guo Q, Sun H. Coordinated dispatch of integrated electric and district heating systems using heterogeneous decomposition. IEEE Trans Sustain Energy 2020;11:1495–507. https://doi.org/10.1109/TSTE.2019.2929183.
[4] Müller FL, Szabó J, Sundström O, Lygeros J. Aggregation and disaggregation of energetic flexibility from distributed energy resources. IEEE Trans Smart Grid 2019;10:1205–14. https://doi.org/10.1109/TSG.2017.2761439.
[5] Rouzbahani HM, Karimipour H, Lei L. A review on virtual power plant for energy management. Sustain Energy Technol Assess 2021;47:101370. https://doi.org/10.1016/j.seta.2021.101370.
[6] Kong X, Xiao J, Wang C, Cui K, Jin Q, Kong D. Bi-level multi-time scale scheduling method based on bidding for multi-operator virtual power plant. Appl Energy 2019;249:178–89. https://doi.org/10.1016/j.apenergy.2019.04.130.
[7] Venegas-Zarama JF, Muñoz-Hernandez JL, Baringo L, Diaz-Cachinero P, De Domingo-Mondejar I. A review of the evolution and main roles of virtual power plants as key stakeholders in power systems. IEEE Access 2022;10:47937–64. https://doi.org/10.1109/ACCESS.2022.3171823.
[8] Wang Y, Li Y, Cao Y, Mohammad S, Jiang L. Optimal operation strategy for multi-energy microgrid participating in auxiliary service. IEEE Trans Smart Grid 2023;14:3523–34. https://doi.org/10.1109/TSG.2023.3250482.
[9] Koraki D, Strunz K. Wind and solar power integration in electricity markets and distribution networks through service-centric virtual power plants. IEEE Trans Power Syst 2018;33:473–85. https://doi.org/10.1109/TPWRS.2017.2710481.
[10] Gao H, Jin T, Feng C, Li C, Chen Q, Kang C. Review of virtual power plant operations: resource coordination and multidimensional interaction. Appl Energy 2024:357. https://doi.org/10.1016/j.apenergy.2023.122284.
[11] Nosratabadi SM, Hooshmand RA, Gholipour E. A comprehensive review on microgrid and virtual power plant concepts employed for distributed energy resources scheduling in power systems. Renew Sust Energ Rev 2017;67:341–63. https://doi.org/10.1016/j.rser.2016.09.025.
[12] Tian L, Chen L, Guo JB, Wang X, Yun Q, Gao W. A review on the study of management and interaction mechanism for distributed energy in virtual power plants. Power Sys Technol 2020;44(6):2097–108. https://doi.org/10.13335/j.1000-3673.pst.2019.2193.
[13] Pal P, Krishnamoorthy PA, Rukmani DK, Antony SJ, Ocheme S, Subramanian U, et al. Optimal dispatch strategy of virtual power plant for day-ahead market framework. Appl Sci 2021;11:3814. https://doi.org/10.3390/app11093814.
[14] Chen Q, Gao H, Feng C, Chen S, Kong X, Kang C. Dynamic construction and trustworthy quantification of virtual power plant: theoretical analysis and key technologies. Automat Electric Power Syst 2022;46:26–36. https://doi.org/10.7500/AEPS20220427008.
[15] Han H, Cui H, Gao S, Shi Q, Fan A, Wu C. A remedial strategic scheduling model for load serving entities considering the interaction between grid-level energy storage and virtual power plants. Energies 2018;11:2420. https://doi.org/10.3390/en11092420.
[16] Bhuiyan EA, Hossain MdZ, Muyeen SM, Fahim SR, Sarker SK, Das SK. Towards next generation virtual power plant: technology review and frameworks. Renew Sust Energ Rev 2021;150:111358. https://doi.org/10.1016/j.rser.2021.111358.
[17] Rahimi M, Ardakani FJ, Ardakani AJ. Optimal stochastic scheduling of electrical and thermal renewable and non-renewable resources in virtual power plant. Int J Electr Power Energy Syst 2021;127:106658. https://doi.org/10.1016/j.ijepes.2020.106658.
[18] Mostafa V-D, Homa R-K, Miadreza S-K, Catalao J. Risk-averse optimal energy and reserve scheduling for virtual power plants incorporating demand response programs. IEEE Trans Smart Grid 2021;12:1405–15. https://doi.org/10.1109/TSG.2020.3026971.
[19] Kang C, Chen Q, Su J, Ai Q, Ji Y, Pan W, et al. Scientific problems and research framework of virtual power plant with enormous flexible distributed energy resources in new power system. Automat Electric Power Syst 2022;46:3–14. https://doi.org/10.7500/AEPS20220401007.
[20] Zahid U, Geev M, Felician C, Yim FH. Comprehensive review of VPPs planning, operation and scheduling considering the uncertainties related to renewable energy sources. IET Energy Syst Integr 2019. https://doi.org/10.1049/iet-esi.2018.0041.
[21] Naval N, Yusta JM. Virtual power plant models and electricity markets - A review. Renew Sust Energ Rev 2021;149:111393. https://doi.org/10.1016/j.rser.2021.111393.
[22] Oluwaseun O, Alvarp O, Lukas S, Luis R, Pedro S-M, Enrique L. Optimal participation of heterogeneous, RES-based virtual power plants in energy markets. Energies 2022;15:3207. https://doi.org/10.3390/en15093207.
[23] Feng C, Wang Y, Wang X, Chen Q. Device access optimization for virtual power plants in heterogeneous networks. IEEE Trans Smart Grid 2022;13:1478–89. https://doi.org/10.1109/TSG.2021.3125042.
[24] Moteza S, Mohammad S-E-E, Haghifam M-R. A medium-term coalition-forming model of heterogeneous DERs for a commercial virtual power plant. Appl Energy 2016;169:663–81. https://doi.org/10.1016/j.apenergy.2016.02.058.
[25] Zhou H, Fan S, Wu Q, Dong L, Li Z, He G. Stimulus-response control strategy based on autonomous decentralized system theory for exploitation of flexibility by virtual power plant. Appl Energy 2021;285:116424. https://doi.org/10.1016/j.apenergy.2020.116424.
[26] Li J, Xu D, Wang J, Zhou B, Wang M, Zhu L. P2P multigrade energy trading for heterogeneous distributed energy resources and flexible demand. IEEE Trans Smart Grid 2023;14:1577–89. https://doi.org/10.1109/TSG.2022.3181703.
[27] Duffaut ELA, Adil K, Mads A. Reference-tracking control policies for packetized coordination of heterogeneous DER populations. IEEE Trans Control Syst Technol 2021;29:2427–43. https://doi.org/10.1109/TCST.2020.3039492.
[28] Yang H, Yu Q, Liu J, Jia Y, Yang G, Ackom E, et al. Optimal wind-solar capacity allocation with coordination of dynamic regulation of hydropower and energy intensive controllable load. IEEE Access 2020;8:110129–39. https://doi.org/10.1109/ACCESS.2020.3001666.
[29] Wu X, Liang K, Han X. Renewable energy output tracking control algorithm based on the temperature control load state-queuing model. Appl Sci-Basel 2018;8:1099. https://doi.org/10.3390/app8071099.
[30] Galvan E, Alcaraz GG, Cabrera NG. Two-phase short-term scheduling of renewable energy resources and demand response. IEEE Latin Am Trans 2015;13:181–7. https://doi.org/10.1109/TLA.2015.7040646.
[31] Sun Y, Wang X, Li Z, Qiu Y, Li B, Wang S, et al. A source load value matching method based on matching degree in different spatial and temporal Scales. In: 2020 7th international conference on information science and control engineering (ICISCE); 2020. p. 1623–6. https://doi.org/10.1109/ICISCE50968.2020.00321.
[32] Liu Y, Qiao Y, Han S, Xu Y, Geng T, Ma T. Quantitative evaluation methods of cluster wind power output volatility and source-load timing matching in regional power grid. Energies 2021;14:5214. https://doi.org/10.3390/en14165214.
[33] Xu W, Ma R, Chen C, Wang W. Day-ahead sharing model of multi-integrated energy service providers based on source-load matching degree. IOP Conf Series: Earth Env Sci 2021;766:012092. https://doi.org/10.1088/1755-1315/766/1/012092.
[34] Gong H, Jones ES, Alden RE, Frye AG, Colliver D. Virtual power plant control for large residential communities using HVAC systems for energy storage. IEEE Trans Ind Appl 2022;58:622–33. https://doi.org/10.1109/TIA.2021.3120971.
[35] Kong X, Wang Z, Liu C, Zhang D, Gao H. Refined peak shaving potential assessment and differentiated decision-making method for user load in virtual power plants. Appl Energy 2023;334:120609. https://doi.org/10.1016/j.apenergy.2022.120609.
[36] Dong W, Wang Q, Yang L. A coordinated dispatching model for a distribution utility and virtual power plants with wind/photovoltaic/hydro generators. Automat Electric Power Syst 2015;39(9):75–81. https://doi.org/10.7500/AEPS20140719007.
[37] Khan R, Islam N, Das SK, Muyeen SM, Moyeen SI. Energy sustainability-survey on technology and control of microgrid, smart grid and virtual power plant. IEEE Acess 2021;9:104663–94. https://doi.org/10.1109/ACCESS.2021.3099941.

[38] Perdichizzi A, Barigozzi G, Franchini G, Ravelli S. Peak shaving strategy through a solar combined cooling and power system in remote hot climate areas. Appl Energy 2015;143:154–63. https://doi.org/10.1016/j.apenergy.2015.01.030.
[39] Ouyang T, Zhang M, Qin P, Tan X. Flow battery energy storage system for microgrid peak shaving based on predictive control algorithm. Appl Energy 2024; 356:122448. https://doi.org/10.1016/j.apenergy.2023.122448.
[40] Luo F, Yang X, Wei W, Zhang T, Yao L. Bi-level load peak shifting and valley filling dispatch model of distribution systems with virtual power plants. Front Energy Res 2021;8. https://doi.org/10.3389/fenrg.2020.596817.
[41] Wang S. Aggregation reference model and quantitative metric system of flexible energy resources. Automat Electric Power Syst 2024;48:1–9. https://doi.org/10.7500/AEPS20230728003.
[42] Carrion M, Arroyo JM. A computationally efficient mixed-integer linear formulation for the thermal unit commitment problem. IEEE Trans Power Syst 2006;21(3):1371–8. https://doi.org/10.1109/TPWRS.2006.876672.
[43] Wang Z, Wang S, Zhang X, Liu W, Gong Q, Chen Q. Load characteristics modeling of regional electric heating system considering difference of users response behaviors. Automat Electric Power Syst 2019;43:63–73. https://doi.org/10.7500/AEPS20180810002.
[44] Hou J, Lin Z, Yang L, Ding Y, Luan K, Yang B. Design of electricity plans for industrial and commercial customers oriented to active demand response on power demand side. Automat Electric Power Syst 2018;42:11–9. https://doi.org/10.7500/AEPS20180404002.
[45] Ren L, Qiu X, Liu B, Han X, Xie J, Sha Y. Optimal dispatching under grid-connection of wind power considering demand response using logit discrete choice model. Power Syst Clean Energy 2017;33:116–24. https://doi.org/10.3969/j.issn.1674-3814.2017.06.020.
[46] Jose A, Philp M, Prasanna LT, Manjula M. Comparison of probit and logistic regression models in the analysis of dichotomous outcomes. Curr Res Biostatistics 2020;10:1–19. https://doi.org/10.3844/amjbsp.2020.
[47] Li J, Ai Q. Operation mode of virtual power plant considering peak regulation auxiliary service. Elect Power Automat Equ 2021;41. https://doi.org/10.16081/j.epae.202103005.
[48] Carrion M, Philpott AB, Conejo AJ, Arroyo JM. A stochastic programming approach to electric energy procurement for large consumers. IEEE Trans Power Syst 2007;22:744–54. https://doi.org/10.1109/TPWRS.2007.895164.
[49] North China energy regulatory bureau of national energy administration of the people's republic of China. Third-party independent entities participate in North China electric power peaking auxiliary service pilot market rules (Trail). 2019. 2019-11-18, https://hbj.nea.gov.cn/dtyw/tzgg/202309/t20230925_120257.html.
[50] East China energy regulatory bureau of national energy administration of the people's republic of China. Shanghai electric power peaking auxiliary service market operation rules (Trail). 2020. 2020-04-22, https://hdj.nea.gov.cn/xxgk/fdzdgknr/jgsx/scjhyjg/202402/t20240210_249027.html.
[51] Taheri SI, Salles MBC, and. Costa E. C. M.. Optimal cost management of distributed generation units and microgrids for virtual power plant scheduling. IEEE. Access 2020;8:208449–61. https://doi.org/10.1109/ACCESS.2020.3039169.
[52] Abdolrasol MGM, Hannan MA, Mohamed A, Amiruldin UAU, Abidin IBZ, Uddin MN. An optimal scheduling controller for virtual power plant and microgrid integration using the binary backtracking search algorithm. IEEE Trans Ind Appl 2018;54(3):2834–44. https://doi.org/10.1109/TIA.2018.2797121.
[53] Neethu EM, Shazia H, Ahmed A, Manohar M. Economic scheduling of virtual power plant in day-ahead and real-time markets considering uncertainties in electrical parameter. Energy Rep 2023;9:3837–50. https://doi.org/10.1016/j.egyr.2023.02.092.